Eur. Phys. J. C (2020) 80:682
https://doi.org/10.1140/epjc/s10052-020-8232-z

THE EUROPEAN PHYSICAL JOURNAL C

Regular Article - Theoretical Physics

Predictions for $B_s \to \bar{K}^* \ell\, \ell$ in non-universal Z' models

Ashutosh Kumar Alok[1,a], **Amol Dighe**[2,b], **Shireen Gangal**[2,c], **Dinesh Kumar**[3,4,d]

[1] Indian Institute of Technology Jodhpur, Jodhpur 342037, India
[2] Tata Institute of Fundamental Research, Mumbai 400005, India
[3] National Centre for Nuclear Research, Pasteura 7, 02-093 Warsaw, Poland
[4] Department of Physics, University of Rajasthan, Jaipur 302004, India

Received: 28 March 2020 / Accepted: 11 July 2020 / Published online: 28 July 2020

Abstract The lepton flavor universality violating (LFUV) measurements R_K and R_{K^*} in B meson decays can be accounted for in non-universal Z' models. We constrain the couplings of these Z' models by performing a global fit to correlated $b \to s\ell\ell$ and $b \to d\ell\ell$ processes, and calculate their possible implications for $B_s \to \bar{K}^*\ell\ell$ observables. For real new physics (NP) couplings, the 1σ favored parameters allow the corresponding LFUV ratio $R^{(s)}_{K^*}$ in $B_s \to \bar{K}^*\ell\ell$ to range between 0.8 and 1.2 at low q^2. Complex NP couplings improve the best fit only marginally, however they allow a significant enhancement of the branching ratio, while increasing the range of $R^{(s)}_{K^*}$ at low q^2 to 0.8–1.8. We find that NP could cause zero-crossing in the forward–backward asymmetry A_{FB} to shift towards lower q^2 values, and enhancement in the magnitude of integrated A_{FB}. The CP asymmetry A_{CP} may be suppressed and even change sign. The simultaneous measurements of integrated $R^{(s)}_{K^*}$ and A_{CP} values to 0.1 and 1% respectively, would help in constraining the effective NP Wilson coefficient C_9 in $b \to d\mu\mu$ interactions.

1 Introduction

In recent times, the most tenacious hints of physics beyond the standard model (SM) have been seen in the decays of B mesons. In particular, there are several measurements in the decays involving the quark-level transition $b \to s\, \ell^+\, \ell^-$ ($l = e,\ \mu$) that deviate from the predictions of SM. These include the LFUV observables R_K and R_{K^*} [1,2] whose measurements disagree with the SM predictions at the level of $\sim 2.5\,\sigma$ [3,4]. This disagreement can be attributed to NP in $b \to s\, e^+\, e^-$ and/or $b \to s\, \mu^+\, \mu^-$ [5–7]. There are also deviations from the SM expectations at the level of $\sim 4\sigma$ in other measurements involving only $b \to s\mu^+\mu^-$ transition, such as the branching ratio of $B_s \to \phi\, \mu^+\, \mu^-$ [8] and angular observable P_5' in $B \to K^*\, \mu^+\, \mu^-$ decay [9–11]. Hence it is natural to try accounting for the discrepancies in all the above measurements by assuming new physics only in the muon sector.

These anomalies may be addressed in a model-agnostic way using the framework of effective field theory, where the effects of NP are incorporated by adding new operators to the SM effective Hamiltonian. Various groups have performed global fits to all available data in the $b \to s\ell^+\ell^-$ sector in order to identify the Lorentz structure of possible new physics operators [12–21]. Some of these new physics operators can be generated in Z' [22–26] or leptoquark models [27–32]. It has been shown that several models with Z', either light or heavy, can help account for the anomalies in $b \to s\mu^+\mu^-$ sector [33–39].

Since the Z' boson would in general couple to all generations, the imprints of such a Z' would be seen in other flavor sectors as well. Therefore, it is worth extending this model to include other related decays. This will provide further insights into the NP flavor structure. In this work, we consider possible observable effects of Z' models on decays induced by the quark-level transition $b \to d\, \mu^+\, \mu^-$.

The $b \to d\mu^+\, \mu^-$ transition gives rise to inclusive semileptonic decays $\bar{B} \to X_d\, \mu^+\, \mu^-$ as well as exclusive semileptonic decays such as $\bar{B} \to (\pi^0,\, \rho)\, \mu^+\, \mu^-$, $B^+ \to \pi^+\, \mu^+\, \mu^-$, and $B_s \to \bar{K}^*\mu^+\mu^-$. Till recently, the only observed decay mode among these was $B^+ \to \pi^+\, \mu^+\, \mu^-$ [40,41], however now LHCb has reported an evidence for the decay $B_s \to \bar{K}^*\mu^+\mu^-$ with a measured branching ratio of $(2.9 \pm 1.1) \times 10^{-8}$ [42]. For other decays, we only have an upper bound on their branching ratios [43,44].

A large number of $b \to d\mu^+\mu^-$ decays, at the level of thousands or tens of thousands, would be observed after the

[a] e-mail: akalok@iitj.ac.in
[b] e-mail: amol@theory.tifr.res.in
[c] e-mail: shireen.gangal@theory.tifr.res.in (corresponding author)
[d] e-mail: dinesh.kumar@ncbj.gov.pl

LHC upgrade. For example, about 17,000 $B^+ \to \pi^+ \mu^+ \mu^-$ events are expected to be observed after collection of the full 300 fb^{-1} dataset. For $B_s \to \bar{K}^* \mu^+ \mu^-$ decays, the full angular analysis is expected to be possible after the LHCb Upgrade-II dataset, where around 4300 events could be observed [45]. This would enable the measurements of angular observables in $B_s \to \bar{K}^* \mu^+ \mu^-$ decays with a precision even better than the existing measurements of angular distributions in $B_d \to K^* \mu^+ \mu^-$ decay.

Currently, as there are not many measurements in the $b \to d$ sector, a model-independent analysis would not be very useful in constraining new physics. However, in the context of specific models (like Z'), some of the couplings can be constrained from the $b \to s$ sector and neutrino trident production. Therefore we choose this approach to constrain the effective couplings in the $b \to d\, \mu^+ \mu^-$ sector, and identify potential observables in the $B_s \to \bar{K}^* \mu^+ \mu^-$ decay where large new physics effects are possible.

The paper is organized as follows. In Sect. 2, we introduce the Z' model considered in this work and indicate how it can be constrained by available measurements. We then describe our fit methodology in Sect. 3. The fit results along with predictions of various $B_s \to \bar{K}^* \mu^+ \mu^-$ observables are presented in Sect. 4. We summarize in Sect. 5.

2 The Z' model and sources of constraints

In the non-universal Z' model that we consider, the Z' boson is associated with a new $U(1)'$ symmetry. It couples to both left-handed and right-handed muons but not to leptons of other generations. It couples to both left-handed and right-handed quarks, however we assume its couplings to right-handed quarks to be flavor-diagonal, thereby avoiding contribution of new chirality flipped operators to flavor changing neutral current (FCNC) decays [46,47]. The change in the Lagrangian density due to the addition of such a heavy Z' boson is

$$\Delta\mathcal{L}_{Z'} = J^\alpha Z'_\alpha, \tag{1}$$

where

$$J^\alpha \supset g_L^{\mu\mu}\, \bar{L}\gamma^\alpha P_L L + g_R^{\mu\mu}\, \bar{L}\gamma^\alpha P_R\, L + g_L^{bd}\, \bar{Q}_1\gamma^\alpha P_L Q_3 + g_L^{bs}\, \bar{Q}_2\gamma^\alpha P_L Q_3 + h.c. \tag{2}$$

The right-hand side in Eq. (2) includes only the terms contributing to FCNC processes. Here $P_{L(R)} = (1 \mp \gamma_5)/2$, Q_i is the i^{th} generation of quark doublet, and $L = (\nu_\mu, \mu)^T$ is the second generation doublet. Further, $g_{L(R)}^{\mu\mu}$ are the left-handed (right-handed) couplings of the Z' boson to muons, and g_L^{bq} to quarks. One can integrate out the heavy Z' and get the relevant terms in the effective four-fermion Hamiltonian as,

$$\begin{aligned}
\mathcal{H}_{\text{eff}}^{Z'} &= \frac{1}{2M_{Z'}^2} J_\alpha J^\alpha \\
&\supset \frac{g_L^{bs}}{M_{Z'}^2} \left(\bar{s}\gamma^\alpha P_L b\right) \left[\bar{\mu}\gamma_\alpha \left(g_L^{\mu\mu} P_L + g_R^{\mu\mu} P_R\right) \mu\right] \\
&\quad + \frac{\left(g_L^{bs}\right)^2}{2M_{Z'}^2} \left(\bar{s}\gamma^\alpha P_L b\right) \left(\bar{s}\gamma_\alpha P_L b\right) \\
&\quad + \frac{g_L^{bd}}{M_{Z'}^2} \left(\bar{d}\gamma^\alpha P_L b\right) \left[\bar{\mu}\gamma_\alpha \left(g_L^{\mu\mu} P_L + g_R^{\mu\mu} P_R\right) \mu\right] \\
&\quad + \frac{\left(g_L^{bd}\right)^2}{2M_{Z'}^2} \left(\bar{d}\gamma^\alpha P_L b\right) \left(\bar{d}\gamma_\alpha P_L b\right) \\
&\quad + \frac{g_L^{\mu\mu}}{M_{Z'}^2} \left(\bar{\nu}_\mu\gamma_\alpha P_L \nu_\mu\right) \left[\bar{\mu}\gamma^\alpha \left(g_L^{\mu\mu} P_L + g_R^{\mu\mu} P_R\right) \mu\right],
\end{aligned} \tag{3}$$

where we have taken the down-type quarks in the quark-doublets Q_i to be in the mass-flavor diagonal basis. In Eq. (3), the first (third) term corresponds to $b \to s(d)\mu^+\mu^-$ transitions, the second (fourth) terms give rise to B_s–$\bar{B}_s$ (B_d–$\bar{B}_d$) mixing, whereas the fifth term contributes to the neutrino trident production $\nu_\mu N \to \nu_\mu N \mu^+\mu^-$ (N = nucleus). Consequently, the products $g_L^{bs} g_{L,R}^{\mu\mu}$ ($g_L^{bd} g_{L,R}^{\mu\mu}$) are constrained by the $b \to s(d)\mu^+\mu^-$ data, and individual magnitudes $|g_L^{bs}|$ ($|g_L^{bd}|$) from the B_s–$\bar{B}_s$ (B_d–$\bar{B}_d$) mixing. The neutrino trident production puts limits on the individual muon couplings $g_{L,R}^{\mu\mu}$. We now discuss constraints on the Z' couplings arising from each of the above measurements.

2.1 $b \to s\,(d)\mu^+\mu^-$ decays

The effective Hamiltonian for $b \to q\mu^+\mu^-$ transition in the SM is

$$\begin{aligned}
\mathcal{H}_{\text{eff}}^{\text{SM}} = -\frac{4G_F}{\sqrt{2}} V_{tq}^* V_{tb} \Bigg[&\sum_{i=1}^{6} C_i \mathcal{O}_i \\
&+ C_7^{bq} \frac{e}{16\pi^2} [\bar{q}\sigma_{\mu\nu}(m_q P_L + m_b P_R) b] F^{\mu\nu} + C_8^{bq} \mathcal{O}_8 \\
&+ C_9^{bq,\text{SM}} \frac{\alpha_{\text{em}}}{4\pi} (\bar{q}\gamma^\mu P_L b)(\bar{\mu}\gamma_\mu \mu) \\
&+ C_{10}^{bq,\text{SM}} \frac{\alpha_{\text{em}}}{4\pi} (\bar{q}\gamma^\mu P_L b)(\bar{\mu}\gamma_\mu\gamma_5 \mu) \Bigg],
\end{aligned} \tag{4}$$

where G_F is the Fermi constant and V_{ij} are the Cabibbo–Kobayashi–Maskawa (CKM) matrix elements. The Wilson coefficients (WC) C_i of the four-fermi operators $\mathcal{O}_i$ encode the short-distance contributions to the Hamiltonian in the SM, where the scale-dependence is implicit, i.e. $C_i \equiv C_i(\mu)$ and $\mathcal{O}_i \equiv \mathcal{O}_i(\mu)$. The operators $\mathcal{O}_i$ ($i = 1, \ldots, 6, 8$) contribute to these processes through the modifications $C_{7,9}(\mu) \to C_{7,9}^{\text{eff}}(\mu, q^2)$, where q^2 is the invariant mass-squared of the final state muon pair. We drop the superscript "eff"

from here on for the sake of brevity. Addition of the new Z' boson to the SM particle spectrum modifies the WCs as $C_{9,10}^{bq} \to C_{9,10}^{bq,\mathrm{SM}} + C_{9,10}^{bq,\mathrm{NP}}$, where

$$C_9^{bq,\mathrm{NP}} = -\frac{\pi}{\sqrt{2}G_F\alpha V_{tb}V_{tq}^*}\frac{g_L^{bq}(g_L^{\mu\mu}+g_R^{\mu\mu})}{M_{Z'}^2},$$
$$C_{10}^{bq,\mathrm{NP}} = \frac{\pi}{\sqrt{2}G_F\alpha V_{tb}V_{tq}^*}\frac{g_L^{bq}(g_L^{\mu\mu}-g_R^{\mu\mu})}{M_{Z'}^2}. \quad (5)$$

In the Z' models, $C_9^{bs,\mathrm{NP}}$ and $C_{10}^{bs,\mathrm{NP}}$ are in general independent. Two of the one-parameter scenarios, $C_{10}^{bs,\mathrm{NP}} = 0$ (popularly known as $C_9^{bs,\mathrm{NP}} < 0$) and $C_9^{bs,\mathrm{NP}} = -C_{10}^{bs,\mathrm{NP}}$, can be realized by substituting $g_L^{\mu\mu} = g_R^{\mu\mu}$ and $g_R^{\mu\mu} = 0$, respectively.

2.2 $B_{s(d)} - \bar{B}_{s(d)}$ mixing

The dominant contribution to $B_q - \bar{B}_q$ mixing within the SM comes from the virtual top quark in the box diagram. The Z' boson contributes to $B_q - \bar{B}_q$ mixing at the tree-level. The combined contribution to M_{12}^q, the dispersive part of the box diagrams responsible for the mixing, is

$$M_{12}^q = \frac{1}{3}M_{B_q}f_{B_q}^2\widehat{B}_{B_q}\left[N\,C_{\mathrm{VLL}}^{\mathrm{SM}} + \frac{\left(g_L^{bq}\right)^2}{2M_{Z'}^2}\right], \quad (6)$$

where

$$N = \frac{G_F^2M_W^2}{16\pi^2}\left(V_{tb}V_{tq}^*\right)^2,$$
$$C_{\mathrm{VLL}}^{\mathrm{SM}} = \eta_B x_t\left[1+\frac{9}{1-x_t}-\frac{6}{(1-x_t)^2}-\frac{6x_t^2\ln x_t}{(1-x_t)^3}\right], \quad (7)$$

with $x_t \equiv m_t^2/M_W^2$. Here η_B=0.84 is the short-distance QCD correction calculated at NNLO [48], f_{B_q} is the decay constant, and $\widehat{B}_{B_q}$ is the bag factor. The mass difference $\Delta M_q = 2|M_{12}^q|$ is

$$\Delta M_q = \Delta M_q^{\mathrm{SM}}\left|1+\frac{\left(g_L^{bq}\right)^2}{2\,N\,C_{\mathrm{VLL}}^{\mathrm{SM}}\,M_{Z'}^2}\right|, \quad (8)$$

while the relevant weak phase ϕ_q is

$$\phi_q = -2\beta_q = \arg(M_{12}^q). \quad (9)$$

2.3 Neutrino trident production

Within the Z' models, the modification of the cross section σ for neutrino trident production, $\nu_\mu N \to \nu_\mu N\mu^+\mu^-$ may be parameterized as [49]

$$R_\nu = \frac{\sigma}{\sigma_{\mathrm{SM}}} = \frac{1}{1+(1+4s_W^2)^2}\left[\left(1+\frac{v^2g_L^{\mu\mu}(g_L^{\mu\mu}-g_R^{\mu\mu})}{M_{Z'}^2}\right)^2 + \left(1+4s_W^2+\frac{v^2g_L^{\mu\mu}(g_L^{\mu\mu}+g_R^{\mu\mu})}{M_{Z'}^2}\right)^2\right], \quad (10)$$

where $v = 246$ GeV and $s_W = \sin\theta_W$.

3 Fit methodology

We now determine favored values of the new physics couplings g_L^{bs}, g_L^{bd}, $g_L^{\mu\mu}$ and $g_R^{\mu\mu}$. We nominally take the mass of the Z' boson to be $M_{Z'} = 1$ TeV. Note that since $M_{Z'}$ only appears through the combination $g^2/M_{Z'}^2$, the constraints on couplings can be appropriately scaled with the actual value of $M_{Z'}$.

In $b \to s\mu^+\mu^-$ decays, we consider the following observables: (i) $B_s \to \mu^+\mu^-$ branching ratio [50–52], (ii) the updated value of R_K by the LHCb collaboration [4], (iii) R_{K^*} measured by LHCb [3] and its new Belle measurements, reported at Moriond'19 [53] (for Belle results, we use measurements in the bins 0.045 GeV^2 $< q^2 <$ 1.1 GeV^2, 1.1 GeV^2 $< q^2 <$ 6.0 GeV^2, and 15.0 GeV^2 $< q^2 <$ 19.0 GeV^2, for B^0 as well as B^+ decays), (iv) the differential branching ratios of $B_d \to K^*\mu^+\mu^-$ [54–57], $B^+ \to K^{*+}\mu^+\mu^-$, $B_d \to K\mu^+\mu^-$, $B^+ \to K^+\mu^+\mu^-$ [55,58], and $B \to X_s\mu^+\mu^-$ [59] in several q^2 bins, (v) various CP-conserving and CP-violating angular observables in $B_d \to K^*\mu^+\mu^-$ [10,55,57,60,61], (vi) the measurements of differential branching ratio and angular observables of $B_s \to \phi\mu^+\mu^-$ [8] in several q^2 bins.

While the ratios R_K and R_{K^*} are theoretically clean, other observables are plagued by sizeable uncertainties mainly coming from form factors. For $B_s \to \phi$ and $B \to K$ decays, we use the most precise form factor predictions obtained in light cone sum rule (LCSR) [62,63], taking into account the correlations between the uncertainties of different form factors and at different q^2 values. The non-factorizable corrections are taken into account following the parameterization used in Ref. [63,64]. These are also compatible with the computations in Ref. [65].

All the observables in the $b \to s\mu^+\mu^-$ sector put constraints on the combinations $g_L^{bs}g_L^{\mu\mu}$ and $g_L^{bs}g_R^{\mu\mu}$. For the fit related to $b \to s\mu^+\mu^-$, we closely follow the methodology of Ref. [13]. The χ^2 function for all the $b \to s\mu^+\mu^-$ observables listed above is calculated as

$$\chi^2_{b\to s\mu\mu}(C_i) = [\mathcal{O}_{\mathrm{th}}(C_i) - \mathcal{O}_{\mathrm{exp}}]^T\mathcal{C}^{-1}[\mathcal{O}_{\mathrm{th}}(C_i) - \mathcal{O}_{\mathrm{exp}}], \quad (11)$$

where $C_i = C_{9,10}^{bs,\mathrm{NP}}$. Here $\mathcal{O}_{\mathrm{th}}(C_i)$ are the theoretical predictions of $b \to s\mu^+\mu^-$ observables calculated using `flavio` [64], and $\mathcal{O}_{\mathrm{exp}}$ are the corresponding experimental measure-

ments. The total covariance matrix $\mathcal{C}$ is obtained by adding the individual theoretical and experimental covariance matrices. In order to get the theoretical uncertainties, including the correlations among them, all input parameters such as the form factors, bag parameters, masses of particles, decay constants etc. are varied assuming a Gaussian distribution, following the same methodology as used in `flavio` [64]. For the experimental covariance, we take into account the correlations among the angular observables in $B \to K^{(*)}\mu^+\mu^-$ [10] and $B_s \to \phi\mu^+\mu^-$ [8]. For the other observables, we add the statistical and systematic errors in quadrature. Wherever the errors are asymmetric, we use the conservative approach of using the larger error on both sides of the central value.

We now turn to $B_q - \bar{B}_q$ mixing. Here we consider constraints from ΔM_d, ΔM_s, and the two CP-violating phases. Using $f_{B_d}\sqrt{\widehat{B}_{B_d}} = (225 \pm 9)$ MeV [66], along with other input parameters from Ref. [67], Eq. (8) gives $\Delta M_d^{\rm SM} = (0.547 \pm 0.046)\,{\rm ps}^{-1}$. With $\Delta M_d^{\rm exp} = (0.5065 \pm 0.0019)\,{\rm ps}^{-1}$ [68], the contribution of ΔM_d to χ^2 is

$$\chi^2_{\Delta M_d} = \left(\frac{\Delta M_d - \Delta M_d^{\rm exp,m}}{\sigma_{\Delta M_d}}\right)^2, \tag{12}$$

where we denote the experimental mean value of an observable X by $X^{\rm exp,m}$, and the uncertainty in the observable by σ_X. In order to obtain σ_X, we add the experimental and theoretical uncertainties in quadrature. Here, $\sigma_{\Delta M_d}$ is dominated by the theoretical uncertainty.

In order to minimize the impact of theoretical uncertainties, we use ΔM_s constraints through the ratio $M_R = \Delta M_d/\Delta M_s$. In the SM,

$$M_R^{\rm SM} = \left|\frac{V_{td}}{V_{ts}}\right|^2 \frac{1}{\xi^2}\frac{M_{B_d}}{M_{B_s}}, \tag{13}$$

where $\xi = \frac{f_{B_d}^2 \widehat{B}_{B_d}}{f_{B_s}^2 \widehat{B}_{B_s}}$. Using $\xi = 1.2014^{+0.0065}_{-0.0072}$ [69] and $|V_{td}/V_{ts}| = 0.2088^{+0.0016}_{-0.0030}$ [70], we obtain $M_R^{\rm SM} = 0.0297 \pm 0.0009$, where we have added the errors in quadrature. Wherever there are asymmetric errors, we take a conservative approach and use the larger of the errors on two sides. The value of $M_R^{\rm exp} = 0.0285 \pm 0.0001$ [68], so the contribution to χ^2 due to this ratio is

$$\chi^2_{M_R} = \left(\frac{M_R - M_R^{\rm exp,m}}{\sigma_{M_R}}\right)^2. \tag{14}$$

The observables ΔM_d and M_R constrain $|g_L^{bs}|$ and $|g_L^{bd}|$.

The CP-violating constraints from $J/\psi\phi$ and $J/\psi K_S$ decays contribute to the χ^2 as

$$\chi^2_{J/\psi\phi} = \left(\frac{S_{J/\psi\phi} - S^{\rm exp,m}_{J/\psi\phi}}{\sigma_{S_{J/\psi\phi}}}\right)^2,$$
$$\chi^2_{J/\psi K_S} = \left(\frac{S_{J/\psi K_S} - S^{\rm exp,m}_{J/\psi K_S}}{\sigma_{S_{J/\psi K_S}}}\right)^2, \tag{15}$$

where $S_{J/\psi\phi} = -\,{\rm Im}[M_{12}^s]/|M_{12}^s|$ and $S_{J/\psi K_S} = {\rm Im}[M_{12}^d]/|M_{12}^d|$. Here we have taken the measurements to be $S^{\rm exp}_{J/\psi\phi} = 0.02 \pm 0.03$ and $S^{\rm exp}_{J/\psi K_S} = 0.69 \pm 0.02$ [67].

For the constraints from neutrino trident production, we use the quantity $R_\nu = \sigma/\sigma_{\rm SM}$, whose theoretical expression is given in Eq. (10). We have taken $R_\nu^{\rm exp} \equiv 0.82 \pm 0.28$ [71,72]. The contribution to the total χ^2 is

$$\chi^2_{\rm trident} = \left(\frac{R_\nu - R_\nu^{\rm exp,m}}{\sigma_{R_\nu}}\right)^2. \tag{16}$$

This observable constraints $g_L^{\mu\mu}$ and $g_R^{\mu\mu}$.

The $b \to d\mu^+\mu^-$ decays are CKM-suppressed as compared to $b \to s\mu^+\mu^-$. In our analysis, we include constraints from the branching ratios of $B^+ \to \pi^+\mu^+\mu^-$ and $B_d \to \mu^+\mu^-$ decays. We do not include the measurements of observables in $B_s \to \bar{K}^*\mu^+\mu^-$ decay in our fit, since we are interested in obtaining predictions for these.

The theoretical expression for $\mathcal{B}(B^+ \to \pi^+\mu^+\mu^-)$ in the Z' model can be obtained from Ref. [73], by adding the NP contribution as given in Eq. (5). The contribution to χ^2 from this decay is

$$\chi^2_{B^+\to\pi\mu\mu} = \left(\frac{\mathcal{B}(B^+ \to \pi\mu\mu) - \mathcal{B}(B^+ \to \pi\mu\mu)^{\rm exp,m}}{\sigma_{\mathcal{B}(B^+\to\pi\mu\mu)}}\right)^2, \tag{17}$$

where $\mathcal{B}(B^+ \to \pi\mu\mu)^{\rm exp} = (1.83 \pm 0.24) \times 10^{-8}$ [41]. Following Ref. [73], a theoretical error of 15% is included due to uncertainties in the $B \to \pi$ form factors [74].

The branching ratio of $B_d \to \mu^+\mu^-$ in our model is given by

$$\mathcal{B}(B_d \to \mu^+\mu^-) = \frac{G_F^2\alpha^2 M_{B_d} m_\mu^2 f_{B_d}^2 \tau_{B_d}}{16\pi^3}|V_{td}V_{tb}^*|^2 \times \sqrt{1 - \frac{4m_\mu^2}{M_{B_d}^2}}\left|C_{10}^{bd,{\rm SM}} + C_{10}^{bd,NP}\right|^2, \tag{18}$$

and the contribution to χ^2 is

$$\chi^2_{B_d\to\mu\mu} = \left(\frac{\mathcal{B}(B_d \to \mu\mu) - \mathcal{B}(B_d \to \mu\mu)^{\rm exp,m}}{\sigma_{\mathcal{B}(B_d\to\mu\mu)}}\right)^2. \tag{19}$$

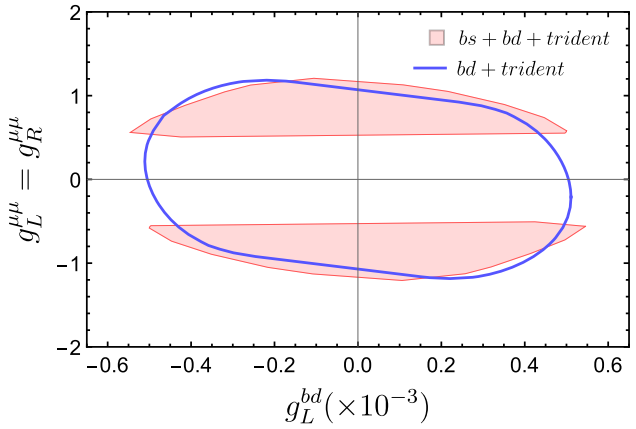

Fig. 1 The $(g_L^{bd},\ g_L^{\mu\mu})$ parameter space corresponding to a Z' model with $g_L^{\mu\mu} = g_R^{\mu\mu}$ (i.e. $C_{10}^{bd,NP} = 0$), for $M_{Z'} = 1$ TeV. The blue curve is the boundary of the 1σ-favored region due to constraints from measurements in $b \to d$ sector and neutrino trident production. The pink shaded region represents the 1σ-favored parameter space after including additional constraints from $b \to s\mu^+\mu^-$ data and $B_s - \bar{B}_s$ mixing

We have used $\mathcal{B}(B_d \to \mu^+\mu^-)^{\rm exp} = (3.9 \pm 1.6) \times 10^{-10}$ [68], $f_{B_d} = (190 \pm 1.3)$MeV [69], and other inputs from [67].

Finally, combining all the above constraints, we obtain

$$\chi^2_{\rm total} = \chi^2_{b\to s\mu\mu} + \chi^2_{\Delta M_d} + \chi^2_{M_R} + \chi^2_{J/\Psi\phi} + \chi^2_{J/\Psi K_S} + \chi^2_{\rm trident} + \chi^2_{B^+\to\pi\mu\mu} + \chi^2_{B_d\to\mu\mu}. \quad (20)$$

In addition to the above constraints, there would be constraints coming from $b \to s\nu\bar{\nu}$ and charm sector. However, at present, we only have upper limits on $b \to s\nu\bar{\nu}$ and $c \to u\mu^+\mu^-$ decays. Further, in the D^0-$\bar{D}^0$ mixing, we expect a large fraction of unknown long-distance contributions. Therefore these measurements cannot be included in as clean a manner as the ones we have considered above. Instead, in the appendices A and B, we determine the allowed regions due to these constraints taken separately and compare with those obtained from our fit. We find that the constraints from these additional channels are much weaker, and will not affect our results.

In the next section, we present our fit results, along with predictions of several observables in $B_s \to \bar{K}^*\mu^+\mu^-$ decay.

4 Fit results and predictions

In a model-independent analysis, there have been attempts to put limits on the new physics couplings for $b \to d\ell\ell$ decays [75], however it is difficult as there are only a few measurements in this sector. Within the context of a Z' model, one can obtain meaningful constraints using correlated $b \to s$ and $b \to d$ processes. This can be seen from Fig. 1, which depicts the allowed $(g_L^{bd},\ g_L^{\mu\mu} = g_R^{\mu\mu})$ parameter space corresponding to a Z' model which generates the 1D scenario $C_{10}^{bd,\rm NP} = 0$. The elliptical region represents the 1σ-favored parameter space with constraints only from $b \to d$ sector, i.e., branching ratios of $B^+ \to \pi^+\mu^+\mu^-$ and $B_d \to \mu^+\mu^-$ decays, $B_d - \bar{B}_d$ mixing, and neutrino trident production. The two shaded regions represent the 1σ-favored parameter space obtained by including additional constraints from all relevant measurements related to $b \to s\mu^+\mu^-$ decays and $B_s - \bar{B}_s$ mixing. It can be seen that the allowed range of NP couplings, in particular $g_{L,R}^{\mu\mu}$, reduces considerably after including constraints from the $b \to s$ sector. Therefore, it is worth studying implications of several measurements in the $b \to s$ sector on the observables in $b \to d\mu^+\mu^-$ decays.

Performing a fit to the relevant observables in $b \to s$ and $b \to d$ sectors, we determine the 1σ-favored parameter space of the couplings g_L^{bd}, g_L^{bs}, $g_L^{\mu\mu}$ and $g_R^{\mu\mu}$, considering g_L^{bs} and g_L^{bd} to be (i) real, (ii) complex. These can be used to find constraints on the NP Wilson coefficients $(C_9^{bd,\rm NP}, C_{10}^{bd,\rm NP})$, and to put limits on the allowed NP in the following observables in $B_s \to \bar{K}^*\mu^+\mu^-$ decay: differential branching ratio, the LFUV ratio $R_{K^*}^{(s)}$, muon forward-backward asymmetry A_{FB}, longitudinal polarization fraction F_L, and direct CP asymmetry A_{CP}.

The matrix element for the decay amplitude of $B_s \to \bar{K}^*\mu^+\mu^-$ can be written as

$$\mathcal{M} = \frac{G_F\alpha}{\sqrt{2}\pi} V_{tb}V_{td}^* \Big\{ \Big[C_9^{bd} \langle \bar{K}^*|\bar{d}\gamma^\mu P_L b|B_s\rangle - \frac{2m_b}{q^2} C_7^{bd} \langle \bar{K}^*|\bar{d}\, i\sigma^{\mu\nu} q_\nu P_R\, b|B_s\rangle \Big] (\bar{\mu}\gamma_\mu\mu) + C_{10}^{bd} \langle \bar{K}^*|\bar{d}\gamma^\mu P_L b|B_s\rangle (\bar{\mu}\gamma_\mu\gamma_5\mu) \Big\}, \quad (21)$$

where $C_9^{bd,\rm SM}$ and $C_{10}^{bd,\rm SM}$ are taken from Ref. [76] and Ref. [77] respectively. The matrix elements appearing in Eq. (21) have been calculated using form factors obtained by a combined fit to lattice calculations and QCD sum rules on the light cone [63]. We also include the non-factorizable corrections due to soft gluon emission and charmonium resonance, which have been computed for $B_d \to K^*\ell\ell$ [65,78], and parameterized as corrections to $C_9^{\rm SM}$. These effects are assumed to be roughly the same for $B_s \to \bar{K}^*\ell\ell$ due to flavor symmetry [79].

The decay $B_s \to \bar{K}^*\mu^+\mu^-$ may be described in terms of the fourfold distribution as [79]

$$\frac{d\,\Gamma}{dq^2} = \int_{-1}^{+1} d\cos\theta_l\, d\cos\theta_V \int_0^\pi d\phi \frac{d^4\Gamma}{dq^2\, d\cos\theta_V\, d\cos\theta_l\, d\phi} = \frac{1}{4}(3\,I_1^c + 6I_1^s - I_2^c - 2I_2^s), \quad (22)$$

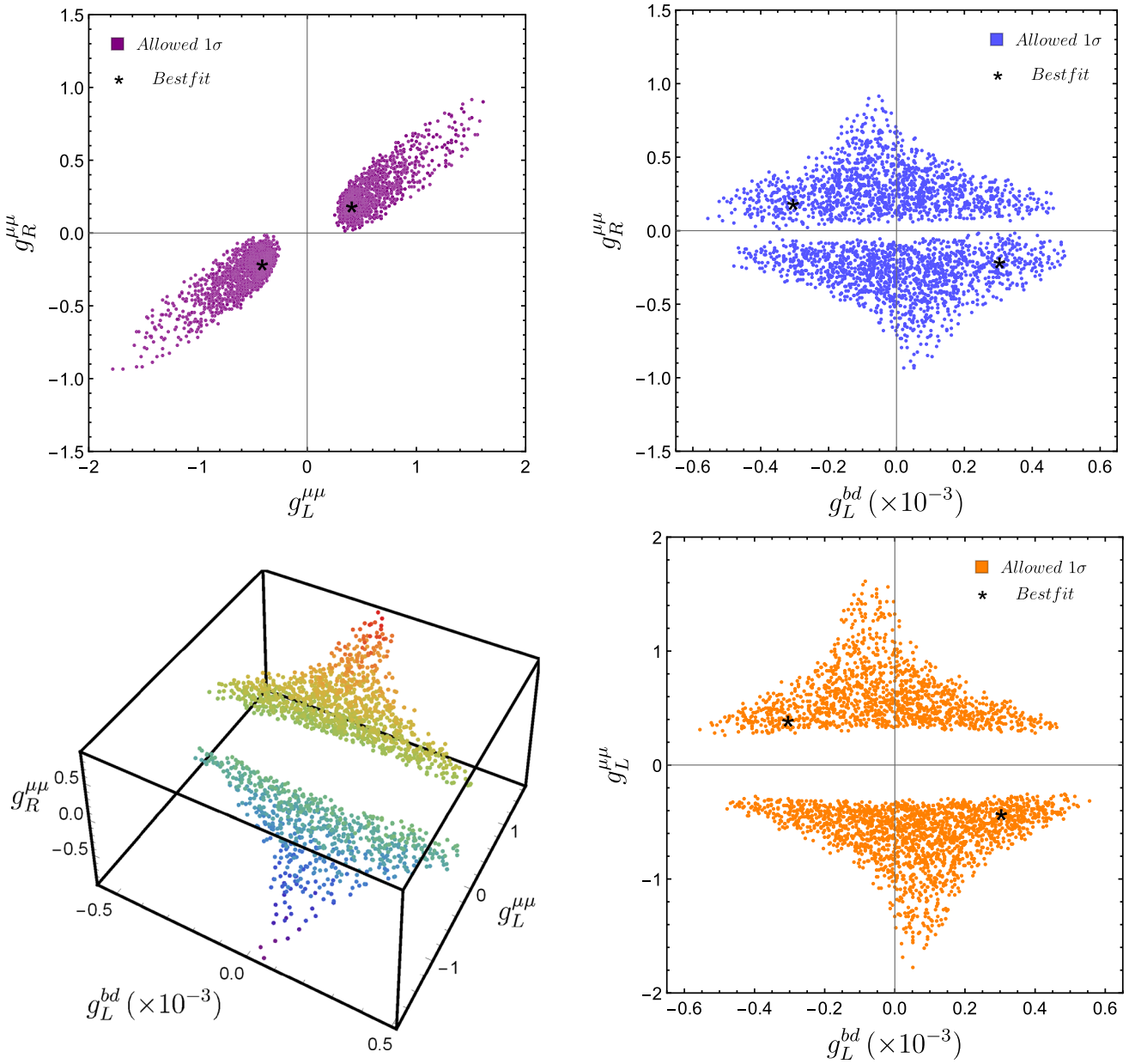

Fig. 2 The 1σ-favored $(g_L^{bd}, g_L^{\mu\mu}, g_R^{\mu\mu})$ parameter space for a Z' model with real couplings, for $M_{Z'} = 1$ TeV. The colors red to blue in the bottom left 3D parameter space correspond to decreasing values of $g_R^{\mu\mu}$

Table 1 Values of NP Wilson coefficients for benchmark scenarios NP1, NP2 corresponding to a Z' model with real couplings, and scenarios NP3, NP4 with complex couplings. The first two benchmark scenarios NP1 and NP2 for real Z' couplings, correspond to a maximum deviation from the SM predictions of the observables considered. The last two scenarios, for complex couplings, are the 1σ-favoured ones with a near-maximum value of $\mathrm{Im}[C_9^{bd,\mathrm{NP}}]$ and a near-minimum value of $\mathrm{Re}[C_{10}^{bd,\mathrm{NP}}]$

Scenario	NP1	NP2	NP3	NP4
$C_9^{bd,\mathrm{NP}}$	$+0.98$	-0.80	$-1.4 + 4.9\,i$	$-0.6 + 0.8\,i$
$C_{10}^{bd,\mathrm{NP}}$	-0.17	$+0.19$	$+0.7 - 2.3\,i$	$+0.2 - 0.2\,i$

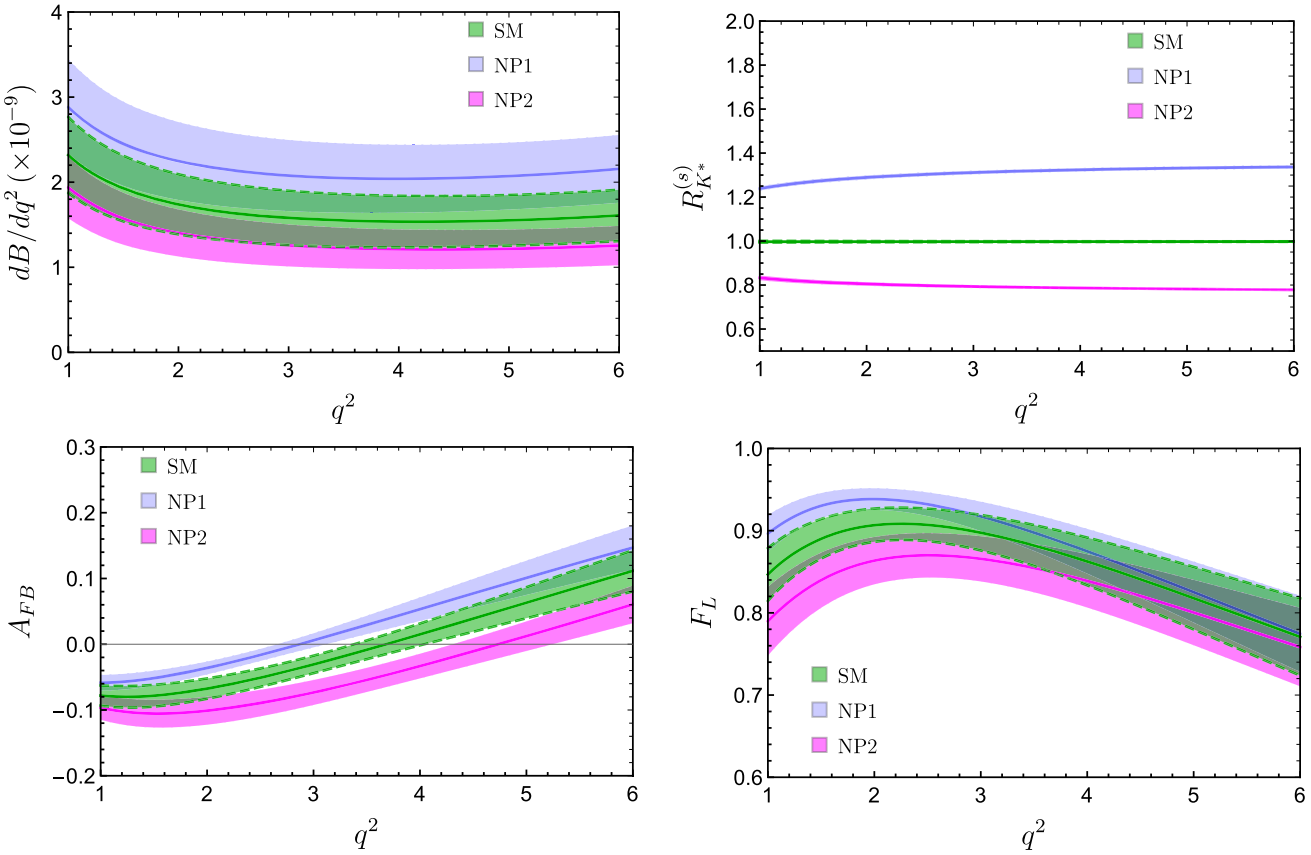

Fig. 3 The predictions for observables in $B_s \to \bar{K}^* \mu^+ \mu^-$ decay, with real Z' couplings, for SM and the benchmark scenarios NP1 and NP2 as in Table 1

where q^2 is the lepton invariant mass, θ_V and θ_l are the polar angles, and ϕ is the angle between the dimuon plane and K^* decay plane. The relevant observables can be obtained from the four-fold distribution as

$$\begin{aligned}
\frac{dB}{dq^2} &= \tau_{B_s} \frac{d\,\Gamma}{d\,q^2}, \\
R_{K^*}^{(s)}(q^2) &= \frac{d\,\Gamma(B_s \to \bar{K}^* \mu^+ \mu^-)/d\,q^2}{d\,\Gamma(B_s \to \bar{K}^* e^+ e^-)/d\,q^2}, \\
A_{FB}(q^2) &= \frac{1}{d\Gamma/dq^2}\Big[\int_{-1}^{0} - \int_{0}^{1}\Big] d\cos\theta_l \frac{d^4\Gamma}{dq^2 d\cos\theta_l} \\
&= \frac{-3I_6^s}{3I_1^c + 6I_1^s - I_2^c - 2I_2^s}, \\
F_L(q^2) &= \frac{3I_1^c - I_2^c}{3I_1^c + 6I_1^s - I_2^c - 2I_2^s}, \\
A_{CP}(q^2) &= \frac{dB/dq^2 - d\bar{B}/dq^2}{dB/dq^2 + d\bar{B}/dq^2},
\end{aligned} \tag{23}$$

where the functions I_i can be expressed in terms of the transversity amplitudes [80]. Here $\bar{B}$ corresponds to the decay mode $\bar{B}_s \to K^* \mu^+ \mu^-$.

We present our results for the above observables at four benchmark NP scenarios as given in Table 1.

4.1 Real couplings

In order to quantify how well the Z' model is able to account for all data in the $b \to s$ and $b \to d$ sectors, we define $\Delta\chi^2 = \chi^2_{\rm SM} - \chi^2_{\rm NP}$, where the minimum χ^2 in the SM, and in the presence of NP Z' couplings, is denoted by $\chi^2_{\rm SM}$ and $\chi^2_{\rm NP}$, respectively. For the case of real couplings, we find the best fit values to be $g_L^{bd} = \pm 0.3 \times 10^{-3}$, $g_L^{\mu\mu} = \mp 0.4$, and $g_R^{\mu\mu} = \mp 0.2$. The value of $\chi^2_{\rm SM} \approx 221$ and $\Delta\chi^2 \approx 41$. The value of $\chi^2_{\rm SM} = 221$ corresponds to $g_L^{bs} = g_L^{bd} = g_L^{\mu\mu} = g_R^{\mu\mu} = 0$. Since allowing all these NP couplings to be non-zero can decrease the χ^2 to $\chi^2_{{\rm NP},(s,d)} \approx 181$, the SM point may be said to be highly disfavoured. However, even if we restrict $g_L^{bd} = 0$, the freedom allowed in the other NP couplings can still allow $\chi^2_{{\rm NP},s} \approx 181$. Thus, the improvement over the SM, $\Delta\chi^2 \approx 41$ is mainly due to the presence of non-zero g_L^{bs} and the muon couplings, which help explain the anomalies in the $b \to s\ell\ell$ sector.

The 1σ-favored parameter space of the couplings (g_L^{bd}, $g_L^{\mu\mu}$, $g_R^{\mu\mu}$) is shown in Fig. 2. It can be seen from (g_L^{bd}, $g_L^{\mu\mu}$)

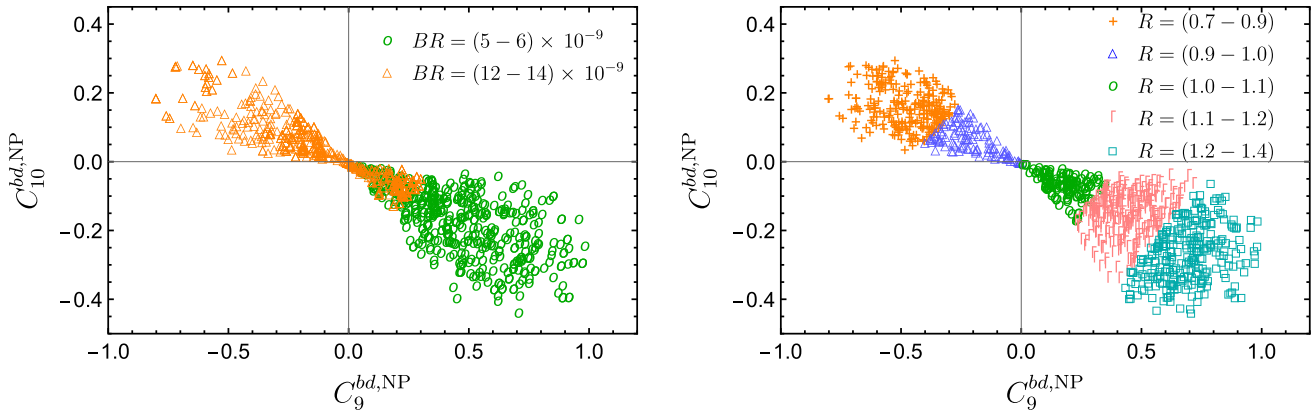

Fig. 4 Integrated values of the branching ratio of $B_s \to \bar{K}^* \mu^+ \mu^-$ (left panel) and the LFUV ratio $R_{K^*}^{(s)}$ (right panel) in the 1σ-favored parameter space of $(C_9^{bd,\mathrm{NP}},\ C_{10}^{bd,\mathrm{NP}})$

and $(g_L^{bd},\ g_R^{\mu\mu})$ planes that, while $g_R^{\mu\mu} = 0$ is barely disfavored within 1σ, a rather wide strip $|g_L^{\mu\mu}| \leq 0.25$ lies beyond the 1σ-favored region. This is because the anomalies in $b \to s\mu\mu$ decays need a non-zero value of $C_9^{bs,\mathrm{NP}}$, which in turn require a non-zero value of $g_L^{\mu\mu}$ or $g_R^{\mu\mu}$. Furthermore, the scenario $C_9^{bs,\mathrm{NP}} = -C_{10}^{bs,\mathrm{NP}}$ [13], which provides a good fit, favors $g_R^{\mu\mu} = 0$, thus requiring $g_L^{\mu\mu}$ to be away from zero. Note that the results in the $(g_L^{\mu\mu}, g_R^{\mu\mu})$ plane indicate the class of favored solutions that lie along $g_L^{\mu\mu} = g_R^{\mu\mu}$, corresponding to $C_{10}^{bs,\mathrm{NP}} \approx 0 \approx C_{10}^{bd,\mathrm{NP}}$.

4.1.1 *Predictions for dB/dq^2, $R_{K^*}^{(s)}(q^2)$, $A_{FB}(q^2)$ and $F_L(q^2)$*

The top left panel of Fig. 3 shows predictions for the differential branching ratio corresponding to real Z' couplings, for the SM as well as two benchmark scenarios NP1 and NP2 from Table. 1. These scenarios roughly correspond to the maximum deviation on either side from the SM predictions in the 1σ favored NP parameter space. The maximum enhancement (suppression) in the differential branching ratio corresponds roughly to a maximum positive (negative) value of $C_9^{bd,\mathrm{NP}}$. It can be seen from the figure that only a marginal enhancement or suppression over the SM value is possible in the differential branching ratio. A clean distinction among the predictions of different scenarios is difficult owing to the large uncertainties (about 20%) arising from the form-factors.

A measurement of the LFUV ratio $R_{K^*}^{(s)}(q^2)$ in a few q^2 bins would be possible with the LHCb upgrade-II data set [45]. The predictions for this quantity in the benchmark scenarios NP1 and NP2 are shown in the top right panel of Fig. 3. In the SM, $R_{K^*}^{(s)}(q^2)$ is unity in the entire low-q^2 region, while an enhancement up to 1.3 and a suppression up to 0.8 is allowed. The maximum enhancement (suppression) roughly corresponds to the maximum positive (negative) value of $C_9^{bd,\mathrm{NP}}$.

Within the SM, the forward-backward asymmetry $A_{FB}(q^2)$ is predicted to vanish around $q^2 \approx 3.5\,\mathrm{GeV}^2$, and the zero-crossing is from negative to positive, as can be seen from the bottom left panel in Fig. 3. The maximum value of $A_{FB}(q^2)$ in the SM is ≈ 10 %. The positive (negative) value of $C_9^{bd,\mathrm{NP}}$ also shifts the zero-crossing towards lower (higher) q^2 value. The integrated value of A_{FB} over $q^2 = (1-6)\,\mathrm{GeV}^2$ bin is (-0.6 ± 1) % within the SM . The predictions for integrated A_{FB} for the benchmark scenarios NP1 and NP2 are (3.1 ± 1.4)% and (-5 ± 1.7)%, respectively.

The predictions for longitudinal polarization fraction $F_L(q^2)$ are shown in the bottom right panel of Fig. 3. Within the SM, the peak value of $F_L(q^2)$ is ≈ 0.9 around $q^2 \approx 1.8$ GeV^2. The shape of $F_L(q^2)$ does not change with NP and only a marginal deviation from SM is allowed for the benchmark NP scenarios considered here.

Thus, in the case of real couplings, $R_{K^*}^{(s)}(q^2)$ is useful to distinguish the predictions of the two benchmark NP scenarios from the SM expectation, while the predictions for the differential branching ratio, $A_{FB}(q^2)$, and $F_L(q^2)$ may not have distinct NP signatures, owing to the large form factor uncertainties.

4.1.2 *Integrated branching ratio and $R_{K^*}^{(s)}$ in the low-q^2 region*

The results obtained for integrated dB/dq^2 and $R_{K^*}^{(s)}(q^2)$ over the $q^2 = (1-6)\,\mathrm{GeV}^2$ bin are presented in Fig. 4. These results are depicted in the $(C_9^{bd,\mathrm{NP}}, C_{10}^{bd,\mathrm{NP}})$ plane, with different colors and symbols indicating the values of integrated branching ratio (left panel) and integrated $R_{K^*}^{(s)}$ (right panel). At each 1σ-favored value of $(C_9^{bd,\mathrm{NP}}, C_{10}^{bd,\mathrm{NP}})$, we vary the values of form factor parameters within their 1σ range [63] with a Gaussian distribution of uncertainties.

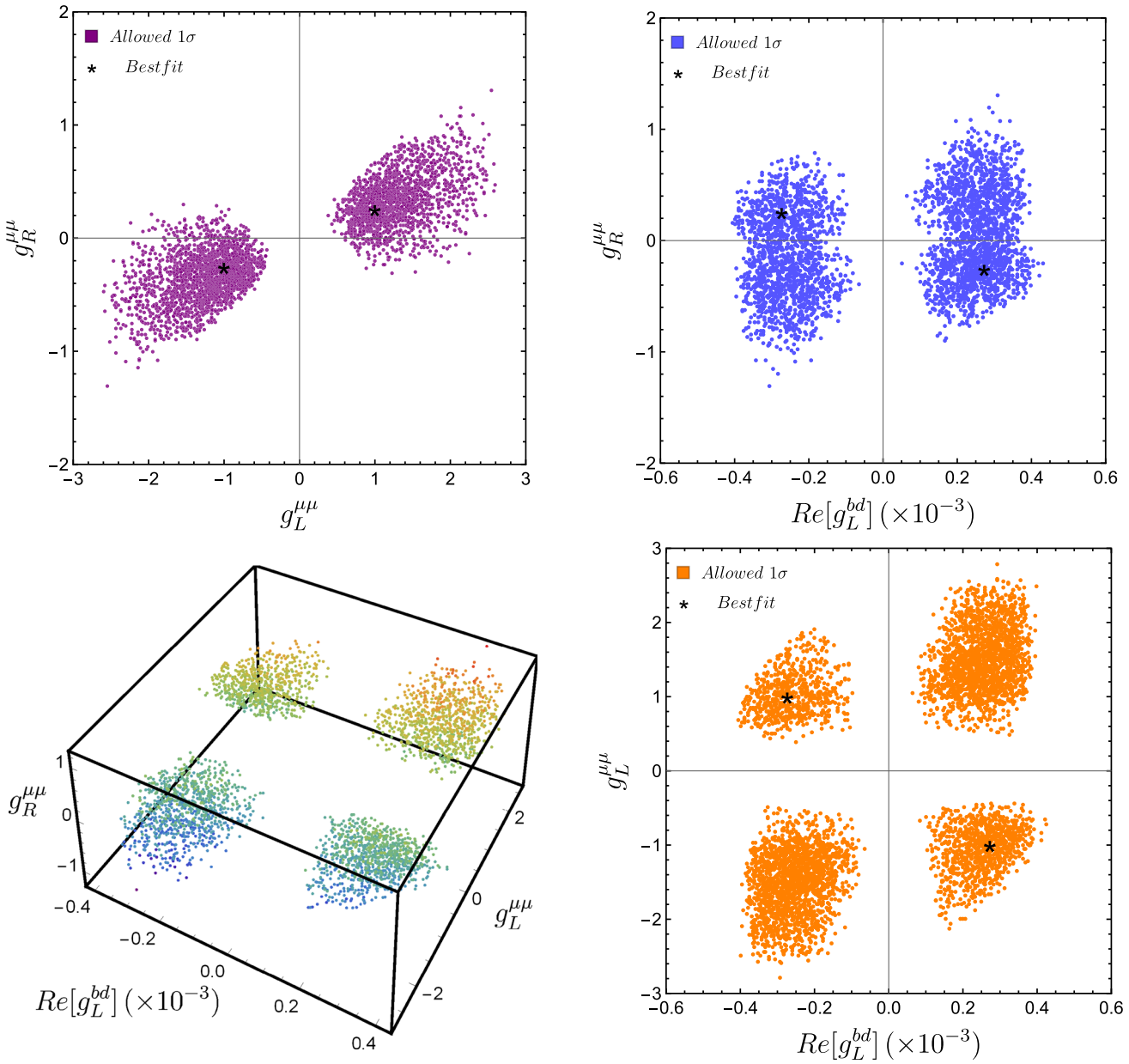

Fig. 5 The 1σ-favored ($\mathrm{Re}[g_L^{bd}]$, $g_L^{\mu\mu}$, $g_R^{\mu\mu}$) parameter space for a Z' model with complex couplings, for $M_{Z'} = 1$ TeV. The colors red to blue in the bottom left 3D parameter space correspond to decreasing values of $g_R^{\mu\mu}$

In the case of integrated branching ratio, the errors due to form factors are about 20%. Due to such large errors, even by considering branching ratio values as different as (5–6) $\times 10^{-9}$ and (12–14) $\times 10^{-9}$, we find a significant overlap in the ($C_9^{bd,\mathrm{NP}}$, $C_{10}^{bd,\mathrm{NP}}$) plane. Hence, a measurement of integrated branching ratio may not be very helpful to put limits on the allowed values of the NP couplings.

In the case of $R_{K*}^{(s)}$, the uncertainties due to form factors cancel in the ratio. The lack of overlap between the regions of integrated $R_{K*}^{(s)}$ values in the range (0.7–1.4) indicates that a future measurement of integrated $R_{K*}^{(s)}$ with an accuracy of $\sim 10\%$ in this decay mode would make it possible to identify the ranges of ($C_9^{bd,\mathrm{NP}}$, $C_{10}^{bd,\mathrm{NP}}$) more precisely. Even with a preliminary measurement, an enhancement in the value of $R_{K*}^{(s)}$ above unity would indicate a positive value of $C_9^{bd,\mathrm{NP}}$ and a negative value of $C_{10}^{bd,\mathrm{NP}}$, while a suppression would imply a negative $C_9^{bd,\mathrm{NP}}$ and positive $C_{10}^{bd,\mathrm{NP}}$. This feature may be understood from the approximate analytic form of the LFUV ratio, $R_{K*}^{(s)} \propto (\mathrm{Re}[C_9^{bq,\mathrm{NP}}] - \mathrm{Re}[C_{10}^{bq,\mathrm{NP}}])$ [81].

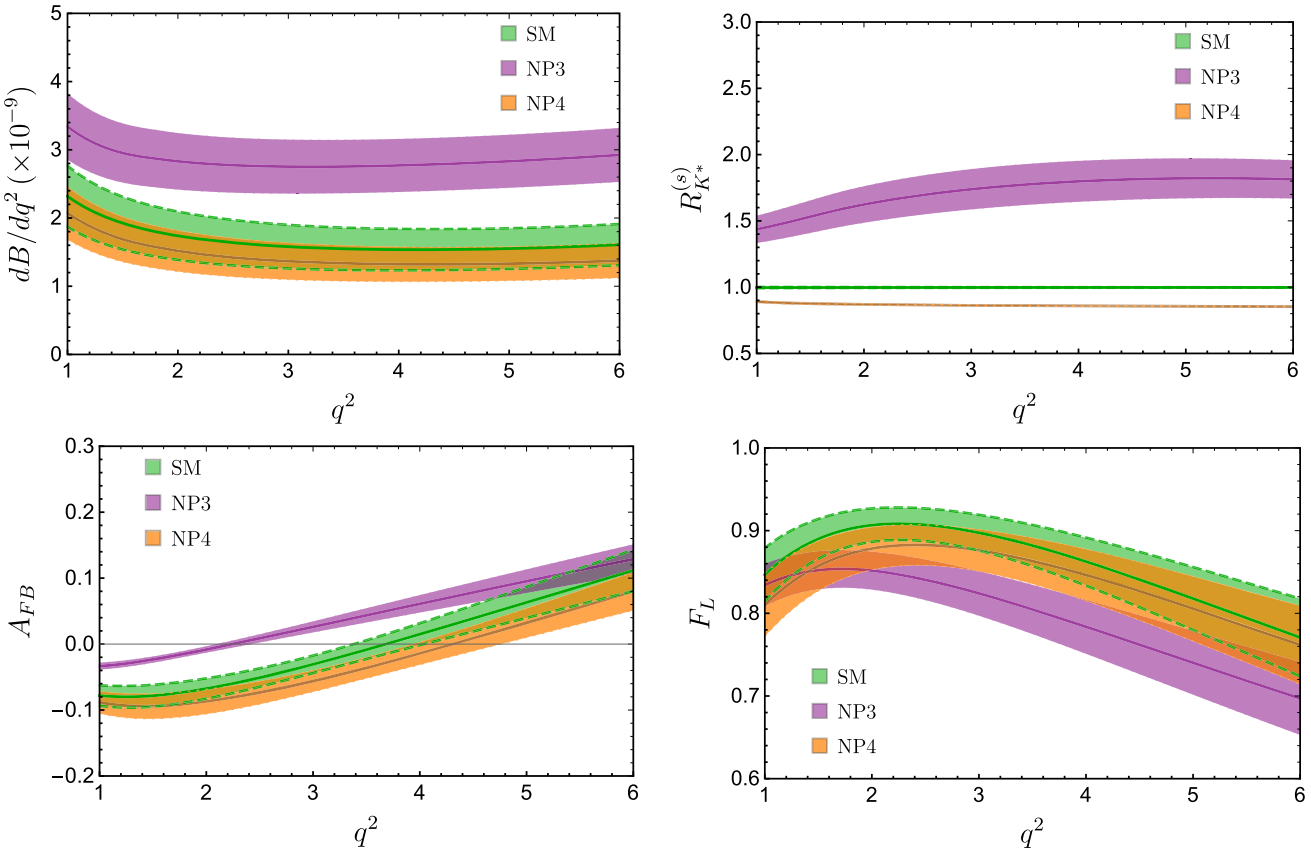

Fig. 6 The predictions for $B_s \to \bar{K}^* \mu^+ \mu^-$ decay, with complex Z' couplings, for SM and the benchmark scenarios NP3 and NP4 as given in Table 1

4.2 Complex couplings

We would now like to see how the predictions for the above observables in the $B_s \to \bar{K}^* \mu^+ \mu^-$ decay would change if the couplings g_L^{bd} and g_L^{bs} are allowed to be complex. Note that since the leptonic current in Eq. (3) is self-conjugate, $g_L^{\mu\mu}$ and $g_R^{\mu\mu}$ must be real. We also study the impact of these complex couplings on the direct CP asymmetry in this decay.

Figure 5 shows the 1σ-favored regions of the couplings $\text{Re}[g_L^{bd}]$, $g_L^{\mu\mu}$, and $g_R^{\mu\mu}$. The minimum χ^2 in the presence of the complex NP couplings is $\chi^2_{\text{NP}} \approx 178$, so that $\Delta\chi^2 \approx 43$, thereby providing a slightly better fit as compared to the case of real couplings ($\Delta\chi^2 = 41$). The corresponding best fit values are $\text{Re}[g_L^{bd}] = \pm 2.7 \times 10^{-3}$, $\text{Im}[g_L^{bd}] = \mp 3.8 \times 10^{-3}$, $g_L^{\mu\mu} = \mp 1$ and $g_R^{\mu\mu} = \mp 0.255$. As χ^2_{NP} for complex couplings is lower compared to that for real couplings, the 1σ-favored parameter space shifts further away from the SM point. A larger parameter space is allowed for the muon couplings compared to the real case, $|g_L^{\mu\mu}| \leq 2.5$ and $|g_R^{\mu\mu}| \leq 1.4$. The 1σ favored region encompasses $g_R^{\mu\mu} = 0$, whereas a rather large region around $g_L^{\mu\mu} = 0$ (i.e. $|g_L^{\mu\mu}| \leq 0.4$) is disfavoured within 1σ. The allowed range of $\text{Im}[g_L^{bd}]$ is qualitatively similar to that of $\text{Re}[g_L^{bd}]$. Note that the complex nature of g_L^{bd} is constrained only from $B_d - \bar{B}_d$ mixing measurements, since no CP-violating measurements are currently available in the $b \to d\mu\mu$ sector.

4.2.1 *Predictions for dB/dq^2, $R^{(s)}_{K^*}(q^2)$, $A_{FB}(q^2)$ and $F_L(q^2)$*

The predictions for differential branching ratio and $R^{(s)}_{K^*}(q^2)$ for the Z' model with complex couplings are shown in the top panel of Fig. 6, for SM as well as the benchmark scenarios NP3 and NP4 in Table 1. These scenarios are the 1σ-favored ones with a maximum value of $\text{Im}[C_9^{bd,\text{NP}}]$ and a minimum value of $\text{Re}[C_9^{bd,\text{NP}}]$, respectively, and are observed to provide close to maximal allowed deviation from the SM predictions. A significant enhancement in the branching ratio is possible in NP3, which could be useful in identifying deviations from the SM. A large enhancement is also possible in the LFUV ratio $R^{(s)}_{K^*}(q^2)$ in the NP3 scenario, with the maximum value of $R^{(s)}_{K^*} = 1.8$ at $q^2 = 6\,\text{GeV}^2$. While the scenario NP4 cannot be distinguished from the SM using only the branching ratio, the value of $R^{(s)}_{K^*}(q^2)$ in this scenario can be as low as 0.85. Therefore, $R^{(s)}_{K^*}(q^2)$ would be useful to identify deviations from the SM.

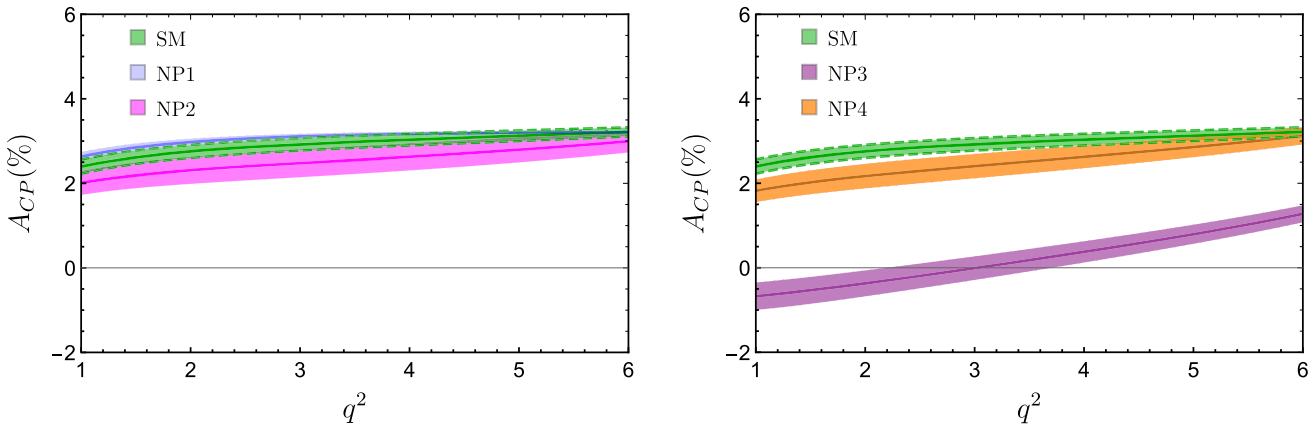

Fig. 7 Predictions for the direct CP asymmetry $A_{CP}(q^2)$ in $B_s \to \bar{K}^* \mu^+ \mu^-$ decay for benchmark scenarios with real couplings (left) and complex couplings (right)

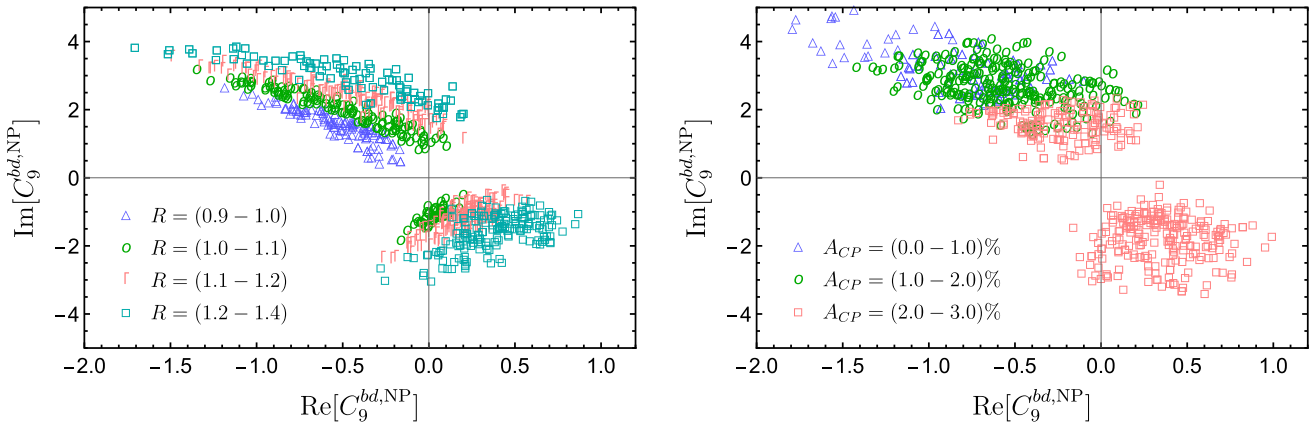

Fig. 8 The integrated values of the LFUV ratio $R_{K^*}^{(s)}$ (left panel) and the direct CP asymmetry A_{CP} (right panel) in the 1σ-favored parameter space of $(\mathrm{Re}[C_9^{bd,\mathrm{NP}}],\ \mathrm{Im}[C_9^{bd,\mathrm{NP}}])$ for the Z' model with complex couplings

A marginal enhancement in $A_{FB}(q^2)$ is possible for the scenario NP3, which would also display zero-crossing at much lower q^2 values ($q^2 \approx 2.5\,\mathrm{GeV}^2$) compared to that in the SM ($q^2 \approx 3.5\,\mathrm{GeV}^2$). A marginal suppression in $F_L(q^2)$ is also possible in NP3. The scenario NP4, on the other hand, does not show significant deviations from the SM for these two observables.

4.2.2 Direct CP asymmetry $A_{CP}(q^2)$

The direct CP asymmetry in the $b \to d\,\mu^+\,\mu^-$ sector is expected to be about an order of magnitude larger than $b \to s\,\mu^+\,\mu^-$. As direct CP violation in $b \to s\,\mu^+\,\mu^-$ sector is expected to be $\sim 0.1\%$, its experimental observation would be possible only if some new physics provides an order of magnitude enhancement to bring it up to the level of a few percent. In $b \to d\,\mu^+\,\mu^-$ decays, the A_{CP} in SM itself is at the level of a few per cent, and can be within experimental reach.

Figure 7 shows $A_{CP}(q^2)$ in the low-q^2 region for the decay $B_s \to \bar{K}^* \mu^+ \mu^-$, considering the benchmark scenarios NP1 and NP2 (real couplings), as well as NP3 and NP4 (complex couplings). It can be seen from the left panel of the figure that for real couplings, $A_{CP}(q^2)$ is either marginally below the SM prediction or almost consistent with it.

For complex couplings, however the suppression in $A_{CP}(q^2)$ can be quite large. It can even lead to $A_{CP}(q^2)$ falling below a per cent level, hence making its measurement extremely difficult. In some scenarios (e.g. NP3), it is even possible for $A_{CP}(q^2)$ to be negative for very low q^2 values. After scanning over the 1σ-favored parameter space, we find no significant enhancement in $A_{CP}(q^2)$. So an NP signal can be established if the measurements put an upper bound which is firmly below the SM prediction of $A_{CP}(q^2)$.

4.2.3 Integrated $R_{K^*}^{(s)}$ and A_{CP}

As observed in the case of real couplings, the integrated branching ratio does not help much in narrowing down the

range of effective NP Wilson coefficients. Hence, in this section, we focus on the integrated values of $R^{(s)}_{K^*}$ and A_{CP} over $q^2 = (1-6)\,\text{GeV}^2$ bin. Figure 8 depicts these results in the (Re[$C_9^{\text{bd,NP}}$], Im[$C_9^{\text{bd,NP}}$]) plane, with different colors and symbols indicating the values of integrated $R^{(s)}_{K^*}$ (left panel) and A_{CP} (right panel). At each 1σ-favored complex value of $(C_9^{bd,\text{NP}}, C_{10}^{bd,\text{NP}})$, we vary the values of form factor parameters within their 1σ range [63] with a Gaussian distribution of uncertainties.

As in the case of real NP couplings, integrated $R^{(s)}_{K^*}$ below the SM prediction of unity could indicate a negative value of Re[$C_9^{bd,\text{NP}}$]. An enhancement in integrated $R^{(s)}_{K^*}$ upto (1.2 - 1.6) is possible for large positive or negative values of Im[$C_9^{bd,\text{NP}}$]. These features may be understood from the observation that in the case of complex couplings, $R^{(s)}_{K^*}$ has contributions both from Re[$C_9^{bd,\text{NP}}$] and $|C_9^{bd,\text{NP}}|^2$.

The right panel of Fig. 8 shows that a large positive value of Im[$C_9^{bd,\text{NP}}$] can decrease the integrated A_{CP} to less than a per cent. The negative values of Im[$C_9^{bd,\text{NP}}$] do not seem to affect A_{CP} much, keeping it close to the SM prediction of 2.5%. Therefore, a simultaneous measurement of integrated $R^{(s)}_{K^*}$ and A_{CP}, with a precision of 0.1 and 1%, respectively, may help identify the sign of Im[$C_9^{bd,\text{NP}}$]. We find that the measurements of integrated $R^{(s)}_{K^*}$ and A_{CP} values are not very useful in identifying the allowed ranges of Re[$C_{10}^{bd,\text{NP}}$] and Im[$C_{10}^{bd,\text{NP}}$].

5 Summary and conclusions

In non-universal Z' models, instrumental in accounting for the flavor anomalies, the observables in $b \to s\ell\ell$ and $b \to d\ell\ell$ processes would be correlated. In this paper, we study the constraints on the couplings of a non-universal Z' model from the measurements in $b \to q\mu\mu$ ($q = s, d$) decays, $B_q - \bar{B}_q$ mixing, and neutrino trident production. These couplings give rise to new additional contributions to the Wilson coefficients C_9^{bq} and C_{10}^{bq}. Using the above constraints, we perform a global fit to determine 1σ-favored regions in the parameter space of the Z' couplings g_L^{bd}, g_L^{bs}, $g_L^{\mu\mu}$, and $g_R^{\mu\mu}$. We analyze the cases when quark-Z' couplings g_L^{bd} and g_L^{bs} are (i) real, and (ii) complex. We also present our predictions for some important observables in $B_s \to \bar{K}^*\mu\mu$ decays — the differential branching ratio dB/dq^2, the LFUV ratio $R^{(s)}_{K^*}$, the angular observables A_{FB} and F_L, and the CP asymmetry A_{CP} — for some benchmark scenarios.

It is observed from our analyses that the Z' model improves the global fit over the SM by $\Delta\chi^2 \approx 41$ (real couplings) and $\Delta\chi^2 \approx 43$ (complex couplings). The favored regions in the parameter space lie along $g_L^{\mu\mu} \approx g_R^{\mu\mu}$, corresponding to $C_{10}^{bd,\text{NP}} \approx 0$, while the region around $g_L^{\mu\mu} = 0$ is disfavored. These are mainly dictated by the R_K and R_{K^*} anomalies in $b \to s$ sector.

For the observables in $B_s \to \bar{K}^*\mu^+\mu^-$ decays, when the couplings are real, we find that the enhancement and suppression in dB/dq^2 cannot be cleanly identified due to the large uncertainties in the SM prediction. However, the value of $R^{(s)}_{K^*}(q^2)$ can substantially deviate from the SM prediction of unity — it can range from 0.8 to 1.3. The enhancement (suppression) corresponds to positive (negative) values of $C_9^{bd,\text{NP}}$. A marginal enhancement and suppression in $A_{FB}(q^2)$ is possible compared to the SM predictions, with the zero-crossing shifting towards lower (higher) q^2 values for positive (negative) values of $C_9^{bd,\text{NP}}$. There is no significant deviation from SM in the predictions of $F_L(q^2)$, and the predictions of $A_{CP}(q^2)$ also stay close to the SM expectation for all the favored values of NP Wilson coefficients. Further, we find that a measurement of integrated $R^{(s)}_{K^*}$ in the low-q^2 bin with a precision of ~ 0.1 can help narrow down the ranges of $(C_9^{bd,\text{NP}}, C_{10}^{bd,\text{NP}})$.

In the case of complex couplings, a larger NP parameter space is allowed, leading to larger possible deviations in the $B_s \to \bar{K}^*\mu\mu$ observables. In particular, a $\sim 50\%$ enhancement in dB/dq^2 is allowed. Moreover, the LFUV ratio $R^{(s)}_{K^*}(q^2)$ can be enhanced up to 1.8 in scenarios with large positive and negative Im[$C_9^{bd,\text{NP}}$]. There can also be a significant enhancement in $A_{FB}(q^2)$ for positive values of Re[$C_9^{bd,\text{NP}}$] and large Im[$C_9^{bd,\text{NP}}$], with the zero-crossing shifting towards lower q^2. A significant suppression in $A_{CP}(q^2)$ compared to the SM prediction of 2.5% is possible for large positive values of Im[$C_9^{bd,\text{NP}}$], which may lead to $A_{CP}(q^2)$ falling below a per cent level. We find that a measurement of integrated $R^{(s)}_{K^*}$ and A_{CP}, with a precision 0.1 and 1%, respectively, would be needed to narrow down the allowed ranges of (Re[$C_9^{bd,\text{NP}}$], Im[$C_9^{bd,\text{NP}}$]).

To summarize, we study NP effects in $B_s \to \bar{K}^*\ell\ell$ decays in a generic Z' model with real as well as complex couplings. The constraints on the Z' couplings are obtained by correlating measurements in the $b \to s$ and $b \to d$ sectors, along with neutrino trident production. We find that

- The present data allow a large deviation (enhancement as well as suppression) in $R^{(s)}_{K^*}$ from its SM prediction. The deviation is more pronounced for complex NP couplings.
- The CP asymmetry can be significantly suppressed as compared to the SM prediction.

The modes $B_s \to \bar{K}^*\ell\ell$ are expected to be measured with a good accuracy in the near future. The observables $R^{(s)}_{K^*}$ and A_{CP} in $B_s \to \bar{K}^*\mu\mu$ decays can show clean signatures of the presence of NP. Hence their measurements will be crucial in the search for physics beyond the SM.

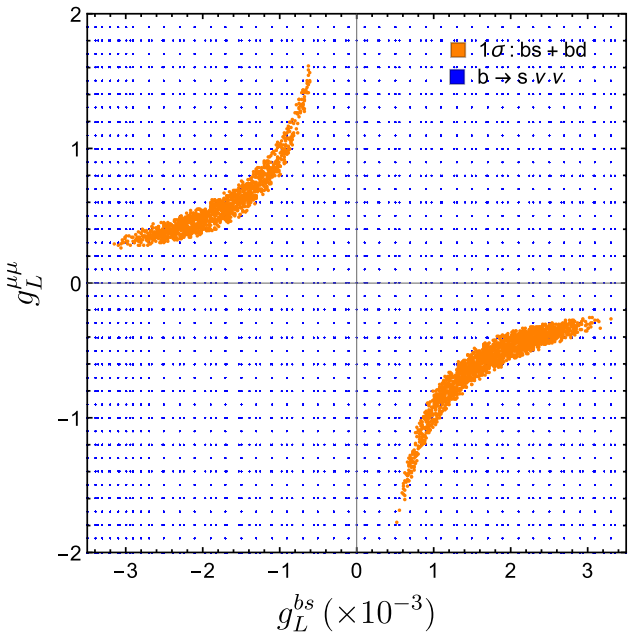

Fig. 9 Comparison of favored NP parameter space using $b \to s\nu\bar{\nu}$ data and combined fit to $b \to s$, $b \to d$ and neutrino trident data

Acknowledgements We would like to thank Suman Kumbhakar for his contribution during the initial stages of this work. The work of DK is supported by the National Science Centre (Poland) under the research Grant no. 2017/26/E/ST2/00470. We would like to thank the organizers of WHEPP 2019, where this work was completed.

Data Availability Statement This manuscript has no associated data or the data will not be deposited. [Authors' comment: This is a theoretical work. The experimental inputs used in our analysis are in the public domain and we have cited the sources of these inputs in the references.]

Funded by SCOAP[3].

Appendix A: Constraints from $b \to s\nu\bar{\nu}$

The quark level transition $b \to s\nu\bar{\nu}$ induces exclusive semileptonic decays $B \to K^{(*)}\nu\nu$. The effective Hamiltonian relevant for $b \to s\nu\bar{\nu}$ transition is [82]

$$H_{\rm eff} = -\frac{\sqrt{2}\alpha G_F}{\pi} V_{tb}V_{ts}^* \sum_\ell C_L^\ell (\bar{s}\gamma_\mu P_L b)(\bar{\nu}_\ell \gamma^\mu P_L \nu_\ell), \tag{A.1}$$

where $C_L^\ell = C_L^{\rm SM} + C_\nu^{\ell\ell}({\rm NP})$. The NP contribution $C_\nu^{\mu\mu}({\rm NP})$ in the Z' model is given by

$$C_\nu^{\mu\mu}({\rm NP}) = -\frac{\pi}{\sqrt{2}G_F\alpha V_{tb}V_{ts}^*}\frac{g_L^{bs}g_L^{\mu\mu}}{M_{Z'}^2}. \tag{A.2}$$

The SM WC is $C_L^{\rm SM} = -X_t/s_W^2$, where $s_W \equiv \sin\theta_W$ and $X_t = 1.469 \pm 0.017$.

From the experimental side, at present, we only have following upper limits [83–87]

$$\begin{aligned}
\mathcal{B}(B^0 \to K^0\nu\bar{\nu}) &< 2.9 \times 10^{-5}\,,\\
\mathcal{B}(B^0 \to K^{*0}\nu\bar{\nu}) &< 2.0 \times 10^{-5}\,,\\
\mathcal{B}(B^+ \to K^+\nu\bar{\nu}) &< 1.7 \times 10^{-5}\,,\\
\mathcal{B}(B^+ \to K^{*+}\nu\bar{\nu}) &< 4.8 \times 10^{-5}.
\end{aligned} \tag{A.3}$$

Using the above bounds, the allowed NP parameter space from $b \to s\nu\bar{\nu}$ data near our best-fit region is depicted in Fig. 9. It is evident that the bounds coming from the current $B \to K^{(*)}\nu\nu$ data are much weaker than those obtained from the combined $b \to s$, $b \to d$ and neutrino-trident fit.

Appendix B: Constraints from D^0-$\bar{D}^0$ mixing and $D^0 \to \mu^+\mu^-$ decay

The quark doublets in Eq. (2) are taken to be in the down-type quark diagonal basis. Hence owing to quark mixing, the up-type quarks in the quark doublets induce $u_i \to u_j$ transitions. Then there can be constraints coming from the up quark sector, in particular D^0-$\bar{D}^0$ mixing and charm decays. The relevant terms in the effective Hamiltonian for the $c \to u$ sector are

$$\begin{aligned}
\mathcal{H}_{\rm eff}^{Z',c\to u} \supset \frac{1}{2M_{Z'}^2} J_\alpha J^\alpha &= \frac{g_L^{cu}}{2M_{Z'}^2}\left(\bar{u}\gamma^\alpha P_L c\right)\left(\bar{u}\gamma_\alpha P_L c\right)\\
&+\frac{h_L^{cu}}{M_{Z'}^2}\left(\bar{u}\gamma^\alpha P_L c\right)\left[\bar{\mu}\gamma_\alpha\left(g_L^{\mu\mu}P_L + g_R^{\mu\mu}P_R\right)\mu\right],
\end{aligned} \tag{B.4}$$

where

$$\begin{aligned}
g_L^{cu} &= \left(g_L^{bs}V_{ud}V_{cb}^*\right)^2 + \left(g_L^{bd}V_{us}V_{cb}^*\right)^2\\
&\quad +2g_L^{bs}g_L^{bd}V_{ud}V_{cb}^*V_{us}V_{cb}^*,\\
h_L^{cu} &= g_L^{bs}V_{ud}V_{cb}^* + g_L^{bd}V_{us}V_{cb}^*.
\end{aligned} \tag{B.5}$$

The first term in Eq. (B.4) induces D^0-$\bar{D}^0$ mixing whereas the second term induces $c \to u\mu^+\mu^-$ transition. Here we consider constraints from D-$\bar{D}$ mixing and $D^0 \to \mu^+\mu^-$.

In the SM, D^0-$\bar{D}^0$ mixing is induced at the loop level by the quarks d, s and b. Due to a strong GIM cancellation, the short-distance contribution is extremely small. In particular, the contribution due to b-quark is highly suppressed, $O(\lambda^8)$. Therefore D^0-$\bar{D}^0$ mixing is dominated by the d- and s-quarks

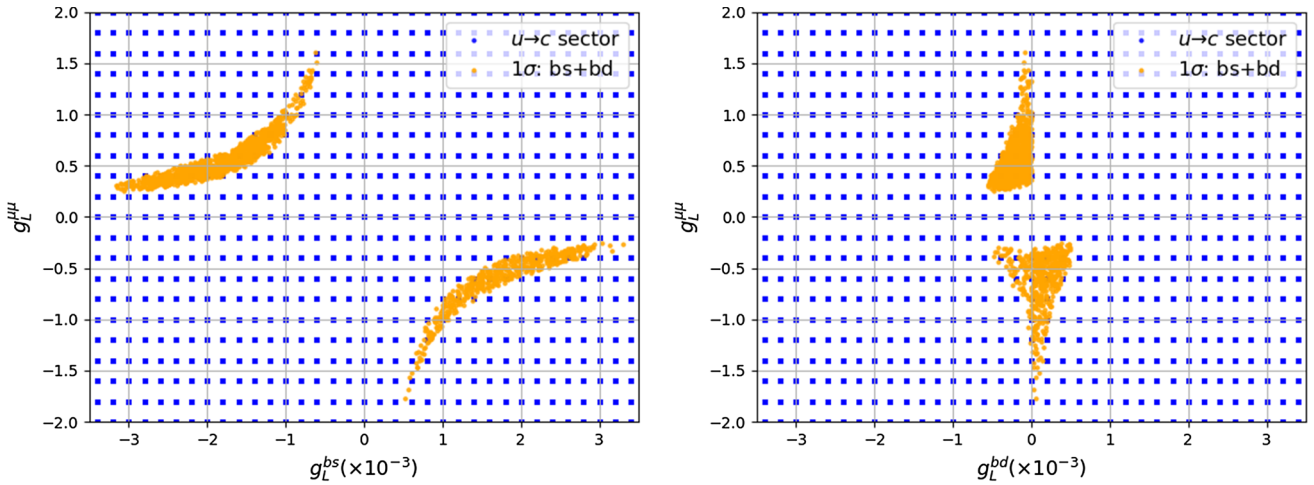

Fig. 10 Comparison of allowed NP parameter space using D^0-$\bar{D^0}$ mixing & branching ratio of $D^0 \to \mu^+\mu^-$ and combined $b \to s$, $b \to d$ and neutrino trident fit

and hence there can be large long-distance contributions, for which there are no reliable estimates at present [88,89]. In our analysis, we consider the D^0-$\bar{D^0}$ mixing parameter ΔM_D which is measured to be $0.0095^{+0.0041}_{-0.0044}$ ps^{-1} [67]. In Z' model, D^0-$\bar{D^0}$ mixing is induced at the tree level and hence would provide a much larger contribution in comparison to the short-distance SM contribution. Further as long-distance contributions are unknown, we saturate the ΔM_D experimental value with new physics contribution which is given by

$$\Delta M_D = \frac{f_D^2\, m_D\, B_D\, r(m_c, M_{Z'})}{3M_{Z'}^2}(g_L^{cu})^2, \tag{B.6}$$

where $f_D = 212.0 \pm 0.7$ MeV [66], $B_D = 0.757 \pm 0.027 \pm 0.004$ [90] and $r(m_c, M_{Z'}) = 0.72$ for $M_{Z'} = 1$ TeV [91].

The decay $D^0 \to \mu^+\mu^-$ is induced by the quark level transition $c \to u\mu^+\mu^-$. In Z' model, the branching ratio is given by

$$B(D^0 \to \mu^+\mu^-) = \frac{\tau_D f_D^2 m_\mu^2 m_D}{32\pi M_{Z'}^4}\sqrt{1-\frac{4m_\mu^2}{m_D^2}} \times (h_L^{cu})^2 (g_L^{\mu\mu} - g_R^{\mu\mu})^2. \tag{B.7}$$

Within the SM, $D^0 \to \mu^+\mu^-$ is dominated by the intermediate $\gamma^*\gamma^*$ state which scales its branching ratio as 2.7×10^{-5} times the branching ratio for $D^0 \to \gamma\gamma$ [92]. Using the upper bound on $D^0 \to \gamma\gamma < 2.2 \times 10^{-6}$ at 90% C.L. [93], the SM branching ratio is estimated to be $\lesssim 10^{-10}$. From the experimental side, we only have an upper bound which is $< 6.2 \times 10^{-9}$ at 90% C.L. [94].

Figure 10 shows the region allowed by the branching ratio of $D^0 \to \mu^+\mu^-$ and ΔM_D as well as from the combined fit in the region around our best-fit point. It is obvious that the constraints coming from the charm sector are significantly weaker.

References

1. G. Hiller, F. Kruger, More model-independent analysis of $b \to s$ processes. Phys. Rev. D **69**, 074020 (2004). arXiv:hep-ph/0310219
2. M. Bordone, G. Isidori and A. Pattori, "On the standard model predictions for R_K and R_{K^*}", Eur. Phys. J. C **76**, no. 8, 440 (2016). arXiv:1605.07633 [hep-ph]
3. R. Aaij et al., [LHCb Collaboration], "Test of lepton universality with $B^0 \to K^{*0}\ell^+\ell^-$ decays". JHEP **1708**, 055 (2017). arXiv:1705.05802 [hep-ex]
4. R. Aaij *et al.* [LHCb Collaboration], "Search for lepton-universality violation in $B^+ \to K^+\ell^+\ell^-$ decays", Phys. Rev. Lett. **122**, no. 19, 191801 (2019). arXiv:1903.09252 [hep-ex]
5. D. Bhatia, S. Chakraborty, A. Dighe, Neutrino mixing and R_K anomaly in U(1)$_X$ models: a bottom-up approach. JHEP **1703**, 117 (2017). arXiv:1701.05825 [hep-ph]
6. B. Capdevila, A. Crivellin, S. Descotes-Genon, J. Matias, J. Virto, Patterns of new physics in $b \to s\ell^+\ell^-$ transitions in the light of recent data. JHEP **1801**, 093 (2018). arXiv:1704.05340 [hep-ph]
7. J. Kumar and D. London, "New physics in $b \to se^+e^-$?". arXiv:1901.04516 [hep-ph]
8. R. Aaij et al., [LHCb Collaboration], "Angular analysis and differential branching fraction of the decay $B_s^0 \to \phi\mu^+\mu^-$". JHEP **1509**, 179 (2015). arXiv:1506.08777 [hep-ex]
9. R. Aaij et al., [LHCb Collaboration], "Measurement of form-factor-independent observables in the decay $B^0 \to K^{*0}\mu^+\mu^-$". Phys. Rev. Lett. **111**, 191801 (2013). arXiv:1308.1707 [hep-ex]
10. R. Aaij et al., [LHCb Collaboration], "Angular analysis of the $B^0 \to K^{*0}\mu^+\mu^-$ decay using 3 fb^{-1} of integrated luminosity". JHEP **1602**, 104 (2016). arXiv:1512.04442 [hep-ex]
11. S. Descotes-Genon, T. Hurth, J. Matias, J. Virto, Optimizing the basis of $B \to K^*ll$ observables in the full kinematic range. JHEP **1305**, 137 (2013). arXiv:1303.5794 [hep-ph]
12. M. Algueró, B. Capdevila, A. Crivellin, S. Descotes-Genon, P. Masjuan, J. Matias and J. Virto, "Emerging patterns of new physics with and without lepton flavour universal contributions". arXiv:1903.09578 [hep-ph]

13. A.K. Alok, A. Dighe, S. Gangal, D. Kumar, Continuing search for new physics in $b \to s\mu\mu$ decays: two operators at a time. JHEP **1906**, 089 (2019). arXiv:1903.09617 [hep-ph]
14. M. Ciuchini, A. M. Coutinho, M. Fedele, E. Franco, A. Paul, L. Silvestrini and M. Valli, "New physics in $b \to s\ell^+\ell^-$ confronts new data on Lepton Universality. arXiv:1903.09632 [hep-ph]
15. G. D'Amico, M. Nardecchia, P. Panci, F. Sannino, A. Strumia, R. Torre, A. Urbano, Flavour anomalies after the R_{K^*} measurement. JHEP **1709**, 010 (2017). arXiv:1704.05438 [hep-ph]
16. A. Datta, J. Kumar and D. London, "The B anomalies and new physics in $b \to se^+e^-$". arXiv:1903.10086 [hep-ph]
17. J. Aebischer, W. Altmannshofer, D. Guadagnoli, M. Reboud, P. Stangl and D. M. Straub, *"B-decay discrepancies after Moriond 2019"*. arXiv:1903.10434 [hep-ph]
18. K. Kowalska, D. Kumar and E. M. Sessolo, "Implications for new physics in $b \to s\mu\mu$ transitions after recent measurements by Belle and LHCb", Eur. Phys. J. C **79**, no. 10, 840 (2019). arXiv:1903.10932 [hep-ph]
19. A. Arbey, T. Hurth, F. Mahmoudi, D. M. Santos and S. Neshatpour, "Update on the $b \to s$ anomalies", Phys. Rev. D **100**, no. 1, 015045 (2019). arXiv:1904.08399 [hep-ph]
20. S. Bhattacharya, A. Biswas, S. Nandi and S. K. Patra, "Exhaustive model selection in $b \to s\ell\ell$ decays: pitting cross-validation against AIC_c". arXiv:1908.04835 [hep-ph]
21. R. Coy, M. Frigerio, F. Mescia and O. Sumensari, "New physics in $b \to s\ell\ell$ transitions at one loop", Eur. Phys. J. C **80**, no. 1, 52 (2020). arXiv:1909.08567 [hep-ph]
22. A. Crivellin, G. D'Ambrosio and J. Heeck, "Addressing the LHC flavor anomalies with horizontal gauge symmetries", Phys. Rev. D **91**, no. 7, 075006 (2015). arXiv:1503.03477 [hep-ph]
23. S.M. Boucenna, A. Celis, J. Fuentes-Martin, A. Vicente, J. Virto, Non-Abelian gauge extensions for B-decay anomalies. Phys. Lett. B **760**, 214 (2016). arXiv:1604.03088 [hep-ph]
24. S.M. Boucenna, A. Celis, J. Fuentes-Martin, A. Vicente, J. Virto, Phenomenology of an $SU(2) \times SU(2) \times U(1)$ model with lepton-flavour non-universality. JHEP **1612**, 059 (2016). arXiv:1608.01349 [hep-ph]
25. W. Altmannshofer, S. Gori, M. Pospelov, I. Yavin, Quark flavor transitions in $L_\mu - L_\tau$ models. Phys. Rev. D **89**, 095033 (2014). arXiv:1403.1269 [hep-ph]
26. L. Darmé, K. Kowalska, L. Roszkowski, E.M. Sessolo, Flavor anomalies and dark matter in SUSY with an extra U(1). JHEP **1810**, 052 (2018). arXiv:1806.06036 [hep-ph]
27. B. Gripaios, M. Nardecchia, S.A. Renner, Composite leptoquarks and anomalies in B-meson decays. JHEP **1505**, 006 (2015). arXiv:1412.1791 [hep-ph]
28. S. Fajfer, N. Košnik, Vector leptoquark resolution of R_K and $R_{D^{(*)}}$ puzzles. Phys. Lett. B **755**, 270 (2016). arXiv:1511.06024 [hep-ph]
29. I. de Medeiros Varzielas and G. Hiller, "Clues for flavor from rare lepton and quark decays", JHEP **1506**, 072 (2015). arXiv:1503.01084 [hep-ph]
30. R. Alonso, B. Grinstein and J. Martin Camalich, "Lepton universality violation and lepton flavor conservation in B-meson decays", JHEP **1510**, 184 (2015). arXiv:1505.05164 [hep-ph]
31. L. Calibbi, A. Crivellin, T. Ota, Effective field theory approach to $b \to sll^{(')}$, $B \to K^{(*)}\nu\bar{\nu}$ and $B \to D^{(*)}\tau\nu$ with Third Generation Couplings. Phys. Rev. Lett. **115**, 181801 (2015). arXiv:1506.02661 [hep-ph]
32. R. Barbieri, G. Isidori, A. Pattori and F. Senia, "Anomalies in B-decays and $U(2)$ flavour symmetry", Eur. Phys. J. C **76**, no. 2, 67 (2016). arXiv:1512.01560 [hep-ph]
33. A. Datta, J. Liao, D. Marfatia, A light Z' for the R_K puzzle and nonstandard neutrino interactions. Phys. Lett. B **768**, 265 (2017). arXiv:1702.01099 [hep-ph]
34. A.J. Buras, J. Girrbach, Left-handed Z' and Z FCNC quark couplings facing new $b \to s\mu^+\mu^-$ data. JHEP **1312**, 009 (2013). arXiv:1309.2466 [hep-ph]
35. D. Aristizabal Sierra, F. Staub and A. Vicente, "Shedding light on the $b \to s$ anomalies with a dark sector" Phys. Rev. D **92**, no. 1, 015001 (2015). arXiv:1503.06077 [hep-ph]
36. B. Allanach, F. S. Queiroz, A. Strumia and S. Sun, "Z' models for the LHCb and $g-2$ muon anomalies", Phys. Rev. D **93**, no. 5, 055045 (2016). arXiv:1511.07447 [hep-ph]
37. L. Calibbi, A. Crivellin, F. Kirk, C. A. Manzari and L. Vernazza, "Z' models with less-minimal flavour violation". arXiv:1910.00014 [hep-ph]
38. Q. Chang, X.Q. Li, Y.D. Yang, $B \to K^* l^+ l^-$, $K l^+ l^-$ decays in a family non-universal Z' model. JHEP **1004**, 052 (2010). arXiv:1002.2758 [hep-ph]
39. Q. Chang, X.Q. Li, Y.D. Yang, A comprehensive analysis of hadronic b $\to$ s transitions in a family non-universal Z-prime model. J. Phys. G **41**, 105002 (2014). arXiv:1312.1302 [hep-ph]
40. R. Aaij et al., [LHCb Collaboration], "First observation of the decay $B^+ \to \pi^+\mu^+\mu^-$". JHEP **1212**, 125 (2012). arXiv:1210.2645 [hep-ex]
41. R. Aaij et al., [LHCb Collaboration], "First measurement of the differential branching fraction and CP asymmetry of the $B^\pm \to \pi^\pm\mu^+\mu^-$ decay". JHEP **1510**, 034 (2015). arXiv:1509.00414 [hep-ex]
42. R. Aaij et al., [LHCb Collaboration], "Evidence for the decay $B_S^0 \to \overline{K}^{*0}\mu^+\mu^-$". JHEP **1807**, 020 (2018). arXiv:1804.07167 [hep-ex]
43. J.-T. Wei et al., [Belle Collaboration], "Search for $B \to \pi l^+ l^-$ Decays at Belle". Phys. Rev. D **78**, 011101 (2008). arXiv:0804.3656 [hep-ex]
44. J. P. Lees *et al.* [BaBar Collaboration], "Search for the rare decays $B \to \pi l^+ l^-$ and $B^0 \to \eta l^+ l^-$", Phys. Rev. D **88**, no. 3, 032012 (2013). arXiv:1303.6010 [hep-ex]
45. A. Cerri *et al.*, "Opportunities in flavour physics at the HL-LHC and HE-LHC". arXiv:1812.07638 [hep-ph]
46. V. Barger, L. Everett, J. Jiang, P. Langacker, T. Liu, C. Wagner, Family non-universal U(1)-prime gauge symmetries and $b \to s$ transitions. Phys. Rev. D **80**, 055008 (2009). arXiv:0902.4507 [hep-ph]
47. V. Barger, L.L. Everett, J. Jiang, P. Langacker, T. Liu, C.E.M. Wagner, $b \to s$ Transitions in family-dependent U(1)-prime models. JHEP **0912**, 048 (2009). arXiv:0906.3745 [hep-ph]
48. G. Buchalla, A.J. Buras, M.E. Lautenbacher, Weak decays beyond leading logarithms. Rev. Mod. Phys. **68**, 1125 (1996). arXiv:hep-ph/9512380
49. A. K. Alok, B. Bhattacharya, D. Kumar, J. Kumar, D. London and S. U. Sankar, "New physics in $b \to s\mu^+\mu^-$: Distinguishing models through CP-violating effects", Phys. Rev. D **96** (2017) no.1, 015034 arXiv:1703.09247 [hep-ph]
50. R. Aaij et al., [LHCb Collaboration], "Measurement of the $B_s^0 \to \mu^+\mu^-$ branching fraction and search for $B^0 \to \mu^+\mu^-$ decays at the LHCb experiment". Phys. Rev. Lett. **111**, 101805 (2013). arXiv:1307.5024 [hep-ex]
51. V. Khachatryan et al., [CMS and LHCb Collaborations], "Observation of the rare $B_s^0 \to \mu^+\mu^-$ decay from the combined analysis of CMS and LHCb data". Nature **522**, 68 (2015). arXiv:1411.4413 [hep-ex]
52. M. Aaboud et al., [ATLAS Collaboration], "Study of the rare decays of B_s^0 and B^0 mesons into muon pairs using data collected during 2015 and 2016 with the ATLAS detector". JHEP **1904**, 098 (2019). arXiv:1812.03017 [hep-ex]
53. A. Abdesselam *et al.* [Belle Collaboration], "Test of lepton flavor universality in $B \to K^*\ell^+\ell^-$ decays at Belle". arXiv:1904.02440 [hep-ex]

54. R. Aaij et al., [LHCb Collaboration], "Measurements of the S-wave fraction in $B^0 \to K^+\pi^-\mu^+\mu^-$ decays and the $B^0 \to K^*(892)^0\mu^+\mu^-$ differential branching fraction". JHEP **1611**, 047 (2016). arXiv:1606.04731 [hep-ex]
55. CDF Collaboration, "Updated branching ratio measurements of exclusive $b \to s\mu^+\mu^-$ decays and angular analysis in $B \to K^{(*)}\mu^+\mu^-$ Decays", CDF public note 10894
56. S. Chatrchyan et al., [CMS Collaboration], "Angular analysis and branching fraction measurement of the decay $B^0 \to K^{*0}\mu^+\mu^-$". Phys. Lett. B **727**, 77 (2013). arXiv:1308.3409 [hep-ex]
57. V. Khachatryan et al., [CMS Collaboration], "Angular analysis of the decay $B^0 \to K^{*0}\mu^+\mu^-$ from pp collisions at $\sqrt{s} = 8$ TeV". Phys. Lett. B **753**, 424 (2016). arXiv:1507.08126 [hep-ex]
58. R. Aaij et al., [LHCb Collaboration], "Differential branching fractions and isospin asymmetries of $B \to K^{(*)}\mu^+\mu^-$ decays". JHEP **1406**, 133 (2014). arXiv:1403.8044 [hep-ex]
59. J.P. Lees et al., [BaBar Collaboration], "Measurement of the $B \to X_s l^+ l^-$ branching fraction and search for direct CP violation from a sum of exclusive final states". Phys. Rev. Lett. **112**, 211802 (2014). arXiv:1312.5364 [hep-ex]
60. M. Aaboud et al., [ATLAS Collaboration], "Angular analysis of $B_d^0 \to K^*\mu^+\mu^-$ decays in pp collisions at $\sqrt{s} = 8$ TeV with the ATLAS detector ". JHEP **1810**, 047 (2018). arXiv:1805.04000 [hep-ex]
61. CMS Collaboration [CMS Collaboration], "Measurement of the P_1 and P_5' angular parameters of the decay $B^0 \to K^{*0}\mu^+\mu^-$ in proton-proton collisions at $\sqrt{s} = 8$ TeV", CMS-PAS-BPH-15-008
62. N. Gubernari, A. Kokulu, D. van Dyk, $B \to P$ and $B \to V$ form factors from B-meson light-cone sum rules beyond leading twist. JHEP **1901**, 150 (2019). arXiv:1811.00983 [hep-ph]
63. A. Bharucha, D.M. Straub, R. Zwicky, $B \to V\ell^+\ell^-$ in the standard model from light-cone sum rules. JHEP **1608**, 098 (2016). arXiv:1503.05534 [hep-ph]
64. D. M. Straub, *"flavio: a Python package for flavour and precision phenomenology in the standard model and beyond"*. arXiv:1810.08132 [hep-ph]
65. A. Khodjamirian, T. Mannel, A.A. Pivovarov, Y.-M. Wang, Charm-loop effect in $B \to K^{(*)}\ell^+\ell^-$ and $B \to K^*\gamma$. JHEP **1009**, 089 (2010). arXiv:1006.4945 [hep-ph]
66. S. Aoki *et al.* [Flavour Lattice Averaging Group], *"FLAG Review 2019"*. arXiv:1902.08191 [hep-lat]
67. M. Tanabashi *et al.* [Particle Data Group], Review of particle physics, Phys. Rev. D **98**, no. 3, 030001 (2018)
68. Y. S. Amhis *et al.* [Heavy Flavor Averaging Group], "Averages of b-hadron, c-hadron, and τ-lepton properties as of 2018". arXiv:1909.12524 [hep-ex]
69. D. King, A. Lenz, T. Rauh, B_s mixing observables and $|V_{td}/V_{ts}|$ from sum rules. JHEP **1905**, 034 (2019). arXiv:1904.00940 [hep-ph]
70. J. Charles *et al.* [CKMfitter Group], "CP violation and the CKM matrix: assessing the impact of the asymmetric B factories", Eur. Phys. J. C **41**, no. 1, 1 (2005) arXiv:hep-ph/0406184
71. S.R. Mishra et al., [CCFR Collaboration], "Neutrino tridents and W Z interference". Phys. Rev. Lett. **66**, 3117 (1991)
72. W. Altmannshofer, S. Gori, J. Martín-Albo, A. Sousa and M. Wallbank, "Neutrino tridents at DUNE". arXiv:1902.06765 [hep-ph]
73. J.J. Wang, R.M. Wang, Y.G. Xu, Y.D. Yang, The rare decays $B_u^+ \to \pi^+ l^+ l^-$, $\rho^+ l^+ l^-$ and $B_d^0 \to l^+ l^-$ in the R-parity violating supersymmetry. Phys. Rev. D **77**, 014017 (2008). arXiv:0711.0321 [hep-ph]
74. P. Ball, R. Zwicky, New results on $B \to \pi, K, \eta$ decay formfactors from light-cone sum rules. Phys. Rev. D **71**, 014015 (2005). arXiv:hep-ph/0406232
75. A. V. Rusov, "Probing new physics in $b \to d$ transitions. arXiv:1911.12819 [hep-ph]
76. A.K. Alok, A. Dighe, S. Ray, CP asymmetry in the decays $B \to (X_s, X_d)\mu^+\mu^-$ with four generations. Phys. Rev. D **79**, 034017 (2009). arXiv:0811.1186 [hep-ph]
77. H.M. Asatrian, K. Bieri, C. Greub, M. Walker, Virtual corrections and bremsstrahlung corrections to $b \to dl^+l^-$ in the standard model. Phys. Rev. D **69**, 074007 (2004). arXiv:hep-ph/0312063
78. S. Descotes-Genon, L. Hofer, J. Matias, J. Virto, Global analysis of $b \to s\ell\ell$ anomalies. JHEP **1606**, 092 (2016). arXiv:1510.04239 [hep-ph]
79. B. Kindra and N. Mahajan, "Predictions of angular observables for $\bar{B}_s \to K^*\ell\ell$ and $\bar{B} \to \rho\ell\ell$ in the standard model", Phys. Rev. D **98**, no. 9, 094012 (2018). arXiv:1803.05876 [hep-ph]
80. W. Altmannshofer, P. Ball, A. Bharucha, A.J. Buras, D.M. Straub, M. Wick, Symmetries and asymmetries of $B \to K^*\mu^+\mu^-$ decays in the standard model and beyond. JHEP **0901**, 019 (2009). arXiv:0811.1214 [hep-ph]
81. G. Hiller, M. Schmaltz, Diagnosing lepton-nonuniversality in $b \to s\ell\ell$. JHEP **1502**, 055 (2015). arXiv:1411.4773 [hep-ph]
82. A.J. Buras, J. Girrbach-Noe, C. Niehoff, D.M. Straub, $B \to K^{(*)}\nu\bar{\nu}$ decays in the standard model and beyond. JHEP **02**, 184 (2015). arXiv:1409.4557 [hep-ph]
83. J. Grygier *et al.* [Belle], "Search for $\boldsymbol{B \to h\nu\bar{\nu}}$ decays with semileptonic tagging at Belle", Phys. Rev. D **96**, no.9, 091101 (2017). arXiv:1702.03224 [hep-ex]
84. J. Lees *et al.* [BaBar], "Search for $B \to K^{(*)}\nu\bar{\nu}$ and invisible quarkonium decays", Phys. Rev. D **87**, no. 11, 112005 (2013). arXiv:1303.7465 [hep-ex]
85. O. Lutz *et al.* [Belle], "Search for $B \to h^{(*)}\nu\bar{\nu}$ with the full Belle $\Upsilon(4S)$ data sample", Phys. Rev. D **87**, no. 11, 111103 (2013). arXiv:1303.3719 [hep-ex]
86. P. del Amo Sanchez *et al.* [BaBar], "Search for the rare decay $B \to K\nu\bar{\nu}$", Phys. Rev. D **82**, 112002 (2010). arXiv:1009.1529 [hep-ex]
87. J. Aebischer, J. Kumar, P. Stangl and D. M. Straub, "A global likelihood for precision constraints and flavour anomalies", Eur. Phys. J. C **79**, no. 6, 509 (2019). arXiv:1810.07698 [hep-ph]
88. A. A. Petrov, Charm mixing in the standard model and beyond, Int. J. Mod. Phys. A **21**, 5686–5693 (2006). arXiv:hep-ph/0611361 [hep-ph]
89. E. Golowich, J. Hewett, S. Pakvasa, A.A. Petrov, Relating D0-anti-D0 mixing and D0 ->l + l- with new physics. Phys. Rev. D **79**, 114030 (2009). arXiv:0903.2830 [hep-ph]
90. N. Carrasco *et al.* [ETM], "S=2 and C=2 bag parameters in the standard model and beyond from $N_f = 2 + 1 + 1$ twisted-mass lattice QCD", Phys. Rev. D **92** (2015) no. 3, 034516. arXiv:1505.06639 [hep-lat]
91. E. Golowich, J. Hewett, S. Pakvasa, A.A. Petrov, Implications of D^0 - $\bar{D}^0$ Mixing for new physics. Phys. Rev. D **76**, 095009 (2007). arXiv:0705.3650 [hep-ph]
92. G. Burdman, E. Golowich, J. L. Hewett, S. Pakvasa, "Rare charm decays in the standard model and beyond", Phys. Rev. D **66**, 014009 (2002). arXiv:hep-ph/0112235 [hep-ph]
93. J. Lees et al., [BaBar], "Search for the decay $D^0 - > \gamma\gamma$ and measurement of the branching fraction for $D^0 - > \pi^0\pi^0$". Phys. Rev. D **85**, 091107 (2012). arXiv:1110.6480 [hep-ex]
94. R. Aaij et al., [LHCb], "Search for the rare decay $D^0 \to \mu^+\mu^-$". Phys. Lett. B **725**, 15–24 (2013). arXiv:1305.5059 [hep-ex]